Modeling and simulation of strain-induced phase transformations under compression and torsion in a rotational diamond anvil cell

Valery I. Levitas[1,2,3,]* and Oleg M. Zarechnyy[2]

[1]*Department of Mechanical Engineering, Iowa State University, Ames, Iowa 50011, USA*

[2]*Department of Aerospace Engineering, Iowa State University, Ames, Iowa 50011, USA*

[3]*Department of Material Science and Engineering, Iowa State University, Ames, Iowa 50011, USA*

Strain-induced phase transformations (PTs) under compression and torsion in rotational diamond anvils are simulated using a finite-element approach. Results are obtained for three ratios of yield strengths of low-pressure and high-pressure phases and are compared with those for the compression without torsion from Levitas and Zarechnyy [Phys. Rev. B **82**, 174123 (2010)]. Various experimental effects are reproduced, including a pressure self-multiplication effect, plateau at pressure distribution at the diffuse interface, simultaneous occurrence of direct and reverse PTs, and irregular stress distribution for PT to a weaker phase. The obtained results change the fundamental understanding of strain-induced PT in terms of interpretation of experimental measurements and the extracting of information on material processes from sample behavior. Intense radial plastic flow moves the high-pressure phase to the low-pressure region, which may lead to misinterpretation of measurements. Various interpretations based on a simplified equilibrium equation (for example, about zero yield strength of phase mixture and hydrostatic conditions during PT) appears to be wrong because of inapplicability of this equation for cases with large gradients of phase concentration and yield strength. The approach developed represents a tool for designing experiments for different purposes and for controlling PTs, and it opens unexpected ways to extract material information by combining simulation and experiment.

I. INTRODUCTION

In Ref. 1, we developed a model and a finite-element approach for studying strain-induced phase transformations (PTs) in rotational diamond anvil cell. The axisymmetric problem of simulation of strain-induced PTs under compression in traditional diamond anvils was solved and various cases were analyzed. Here, we will apply the same model for the solution of three-dimensional (3D) problems of simulation of strain-induced PTs under compression and torsion in rotational diamond anvils, which are usually utilized for studying the effect of plastic shear on high-pressure PTs. The paper is organized as follows. In Sec. II, problem formulation, including boundary conditions, is presented. In Sec. III, solutions for three different ratios of the compressive yield strength of the high-pressure phase to that of the low-pressure phase, σ_{y2}/σ_{y1}, equal to 1, 5, and 0.2, are described and analyzed. In Sec. IV, the PT kinetics, stress tensor, and plastic strain fields for the cases under compression and compression with torsion are compared for the same ratios of the yield strengths. Comparison with a simplified model is presented in Sec. V, and comparison with and interpretation of available experimental data can be found in Sec. VI. Section VII contains concluding remarks.

II. PROBLEM FORMULATION

The problem formulation is very similar to that for the case without PTs (Refs. 2 and 3) and with PT under compression.[1] The axisymmetric geometry of an anvil and sample as well as axisymmetric problem formulation in a cylindrical coordinate system $rz\phi$ will be utilized, along with 3D loading. Due to symmetry with respect to the plane $z=0$ passing through the center of a sample, a quarter of a cross section of a sample before deformation is shown in Fig. 1(b). The initial thickness of a sample between the flat diamond surface $H_0=0.2R$, where R is the anvil radius; the initial thickness of the free part of the sample $H=2H_0$. To avoid any influence of the edge of the sample, the external radius of the sample is chosen as $3R$. The sample is compressed by the increasing axial force Q and then the torsion of an anvil by an angle φ with respect to another anvil was applied under Q=constant. Initial values of all stresses, strains, concentration of the high-pressure phase, and displacements are chosen to be zero. The following boundary conditions are applied [Fig. 1(c)]: (1) at the axis OB ($r=0$), the radial shear stress $\tau_{zr}=0$ and radial displacement $u_r=0$. (2) At the plane of symmetry BC $z=0$, the radial shear stress $\tau_{zr}=0$, the axial displacements $u_z=0$, and the twisting displacements $u_\phi=0$. (3) At the contact surface OKD between rigid diamond and compressed material, all displacements of the sample are equal to the displacement of the anvil, i.e., complete cohesion between anvil and sample is assumed. Compressive axial force Q increasing from zero to the final value was applied to the rigid anvil and was kept constant during rotation of an anvil (and consequently a sample) by an angle $\varphi/2$ with respect to symmetry plane $z=0$. The cohesion condition along the rigid surface OKD results in the condition that axial displacement u_z and rotation angle $\varphi/2$ are the same for each point of the sample's contact surface, and radial displacement $u_r=0$. (4) At the deformed free surfaces DM and MN, the traction vector $t_n=0$.

Below, we analyze the complete cohesion condition.[3] When the pressure exceeds $2\sigma_y$, asperities of the diamond
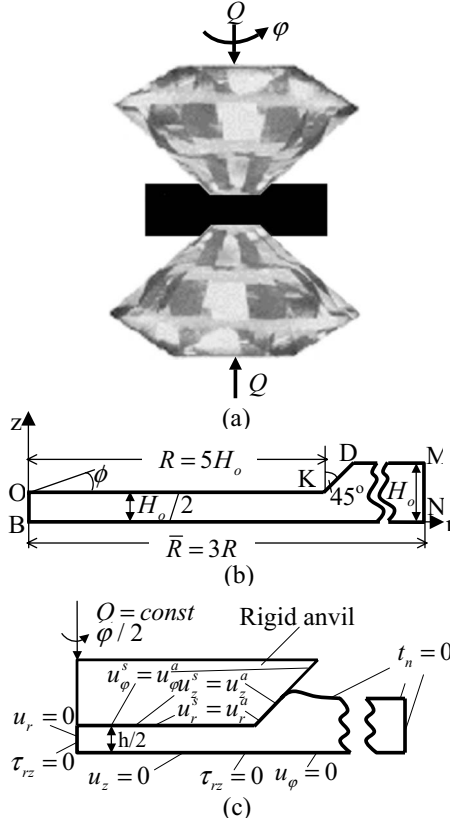
FIG. 1. Geometry of quarter of a sample with boundary conditions.

penetrate into a deformed sample, which leads to complete cohesion between diamond and sample. However, when the magnitude of the shear friction stress, τ, along the sample-anvil interface, $\tau = \sqrt{\tau_{rz}^2 + \tau_{r\phi}^2}$, reaches the yield strength in shear of the two-phase mixture, $\tau_y(c) = \sigma_y(c)/\sqrt{3}$ (according to the von Mises yield condition), the relative sliding is localized just below the contact surface within a thin layer of a sample material. Here, c is the volume fraction of the high-pressure phase and the yield stress in compression of the two-phase mixture is $\sigma_y(c) = (1-c)\sigma_{y1} + c\sigma_{y2}$. This is equivalent to the following sliding condition in the immediate vicinity of the contact surface:

$$\frac{\boldsymbol{v}}{|\boldsymbol{v}|} = \frac{\boldsymbol{\tau}}{\tau} \quad \text{for} \ \tau = \tau_y(c), \quad \boldsymbol{v} = 0 \quad \text{for} \ \tau < \tau_y(c). \quad (1)$$

Here, $\boldsymbol{v}$ is the vector of particles velocity along the contact surface. In Eq. (1), the collinearity of $\boldsymbol{v}$ and $\boldsymbol{\tau}$ is a consequence of isotropy of the plasticity condition. Equation (1) is the particular case of the general contact sliding equation for an anisotropic material.[4] The large elastoplastic deformation and coupled thermomechanical subroutines of the finite-element method (FEM), and the FEM code ABAQUS was implemented in a way similar to that in Ref. 1. All stresses are normalized by the yield strength in the compression of the low-pressure phase σ_{y1}, e.g., $\bar{\sigma}_{zz} = \sigma_{zz}/\sigma_{y1}$ and $\bar{p} = p/\sigma_{y1}$. Dimensional applied axial force is defined as $F = Q/(S\sigma_{y1})$ with S for the initial contact area OKD between an anvil and a sample. For convenience, in figures shear stresses are di-

vided by the yield strength in shear $\tau_{y1} = \sigma_{y1}/\sqrt{3}$, e.g., $\bar{\tau}_{rz} = \tau_{rz}/\tau_{y1}$. The same dimensionless material parameters as in Ref. 1 were utilized in calculations: $\bar{\varepsilon}_t = 0.1$, Young's modulus $E = 162.5$, Poison's ratio $\nu = 0.3$, $p_\varepsilon^d = 6.75$, $p_\varepsilon^r = 6.375$, $p_h^d = 11.25$, $p_h^r = 1.875$, and $a_{ij} = 0.1$. Note that contour lines of equal values of the normal stresses σ_{zz} and σ_{rr} and shear stresses τ_{rz} and $\tau_{r\phi}$, as well as distributions of the normal stresses σ_{zz} and σ_{rr} along the flat contact surface are presented in supplementary material.[5]

III. PHASE TRANSFORMATIONS UNDER TORSION AT CONSTANT AXIAL FORCE

A. Phase transformations for the case with equal yield strengths of phases

We will discuss PTs under torsion at constant axial force $F = 4.44$ after compression for $\sigma_{y2} = \sigma_{y1}$, see Figs. 2 and 3. The thickness of the sample significantly reduces during torsion (see also Fig. 14), which increases the accumulated plastic strain q in addition to torsion. The maximum q is concentrated at the contact surface and strongly grows with growing radius. An increase in the angle of rotation from $\varphi = 0$ to $\varphi = 0.04$ and then to $\varphi = 1.58$ leads to the increase in the maximum value of q from 3.2 to 9.4 and then to 151.8. While the value of accumulated plastic strain is much higher at the surface of the sample than in the middle of the sample, PT will not start until the pressure reaches the minimum pressure p_ε^d for direct PT. Excluding the central region of a sample, pressure grows practically linearly along the radius of the sample from the edge toward the center and does not change appreciably during rotation [similar to the case without PTs (Ref. 3)].

In all figures with pressure fields in a sample [see, e.g., Fig. 2(c)] pressure range $p_\varepsilon^r < p < p_\varepsilon^d$, in which neither direct nor reverse PTs are possible, is shown in magenta. The contours of this region are also shown in all other figures with concentration fields in a sample. In the region to the left of the magenta region, where pressure $p > p_\varepsilon^d$, direct PT occurs; in the region with $p < p_\varepsilon^r$, the reverse PT takes place. In contrast to the compression stage, torsion leads to significant radial flow of a newly formed high-pressure phase into the region with $p < p_\varepsilon^r$, where reverse PT takes place; even a completely transformed high-pressure phase is visible in the region with $p < p_\varepsilon^r$ in Fig. 2(a). Thus, both direct and reverse PTs occur simultaneously in different parts of a sample. Also, *since a high-pressure phase can be experimentally found in the region well below p_ε^d*, a wrong conclusion about a significant (larger than in reality) reduction in PT pressure can be drawn. This is especially important if the kinetics of the reverse strain-induced PT is much slower than that for the direct PT [e.g., as in the case with PT between the graphite-like and superhard phases of boron nitride (BN)].

After compression, a small amount of the high-pressure phase appeared in the center of a sample [Figs. 2(a) and 3(b)]. During torsion, the second maximum in c appears at the surface of the sample and PT completes in these two regions. Then PT completes between these regions and also propagates to the periphery of a sample. The effect of radial flow can be further elaborated if we compare Figs. 2(a) and
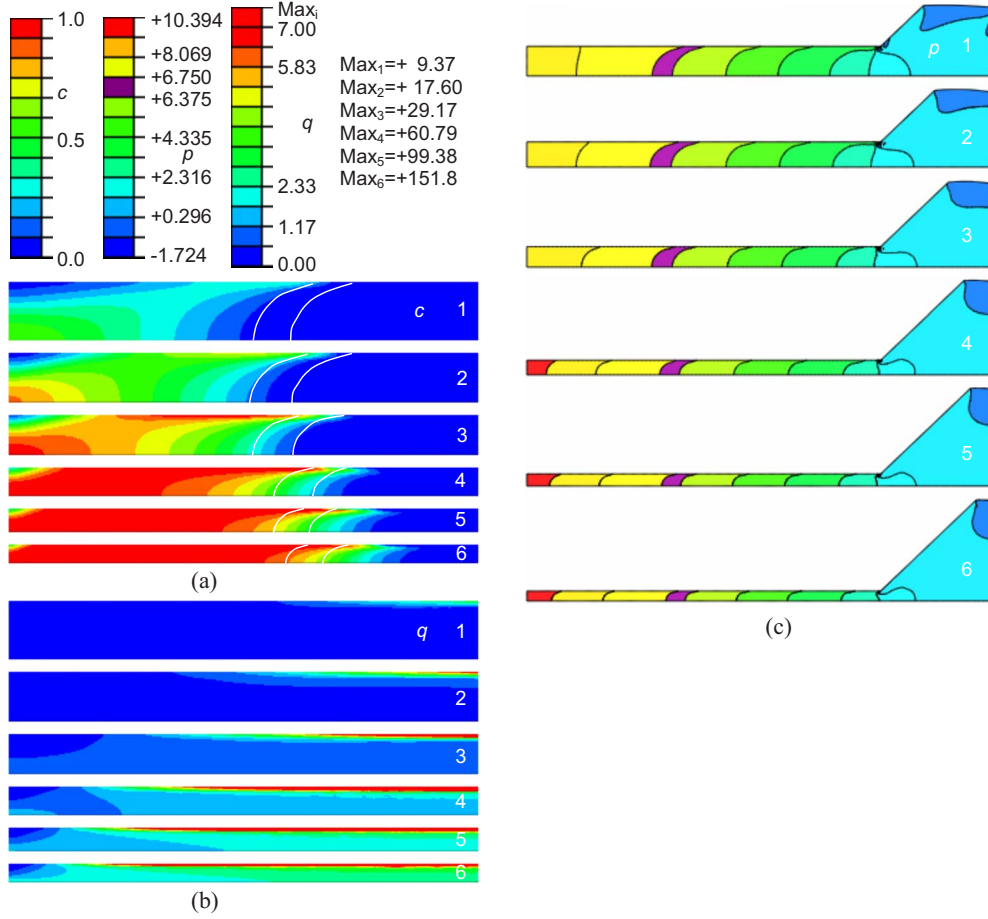
FIG. 2. (Color online) (a) Distributions of concentration of high-pressure phase c, (b) accumulated plastic strain q, and (c) pressure p in a quarter of a cross section of the sample for the case with $\sigma_{2y} = \sigma_{1y}$ for dimensionless applied axial force $F = 4.44$ and different values of angle of rotation φ. Pressure range $p^r_\varepsilon < p < p^d_\varepsilon$ is shown in magenta. The contours of this region are duplicated in Fig. 2(a), for concentration, similar to all other figures with concentration fields in a sample. Maximum values of accumulated plastic strain q for each of six compression stages are shown near color legend. The same is shown in all other figures with pressure and accumulated plastic strain fields in a sample. 1: $\varphi = 0.04$, 2: $\varphi = 0.14$, 3: $\varphi = 0.34$, 4: $\varphi = 0.78$, 5: $\varphi = 1.16$, and 6: $\varphi = 1.58$.

3(b) in the region near the contact surface. It follows from Fig. 3(b) that the evolution of distribution $c(r)$ occurs in the same region where $p > p^d_\varepsilon$ because pressure does not change essentially and radial displacement is prohibited at the contact surface. The concentration c grows, reaches 1, and then the region of complete high-pressure phase spreads in both directions, forming quite sharp interfaces. At the same time, Fig. 2(a) demonstrates that the region with complete PT just below the contact surface, significantly moved to the periphery of a sample (where pressure is well below that of p^d_ε and p^r_ε), because of significant shear strain and displacement localization below the contact surface. Thus, while analysis of $p(r)$ and c distributions along the contact surface may lead to the conclusion that at a diffuse interface the pressure corresponds to the range between p^d_ε and p^r_ε (which can be used for experimental determination of these parameters), distribution of the same fields in the sample volume shows that this is not the case at all. If the high-pressure phase has a different color (as in for BN and KCl), visible interface corresponds to Fig. 2(a) and does not correlates with the region where $p^d_\varepsilon > p > p^r_\varepsilon$. Thus, since pressure distribution does not show any plateau or other signatures of PT, it is very difficult

to determine kinetic parameters p^d_ε and p^r_ε from experiment for this case.

During torsion, torsional shear stress $\tau_{r\phi}$ increases, almost homogeneously for $0.4 < r/R < 1$ at the initial stages of rotation of an anvil, then the homogeneous region spreads almost over the entire contact surface, excluding the small central part [Fig. 3(d)]. In fact, $\tau_{r\phi}$ is getting quite homogeneous along the z coordinate as well [Fig. S1d]. Radial shear stress τ_{zr} along the most part of the contact surface decreases with the increasing of the angle of rotation. This is because the magnitude of friction shear stress vector $\tau = \sqrt{\tau^2_{r\phi} + \tau^2_{zr}}$ reached the yield strength in shear τ_y and the increase in shear twisting stress $\tau_{r\varphi}$ implies the reduction in τ_{zr} [Fig. 3(c)]. Only in the small region near the sample center, where $\tau < \tau_y$ does τ_{zr} grow with growing rotation, causing a small increase in pressure.

To summarize, the most important result in this section is as follows. Significant reduction in thickness of the sample during torsion with a practically unchanged pressure field leads to intense radial plastic flow that moves the high-pressure phase in the region with pressure below p^d_ε and even p^r_ε. Thus, simultaneous direct and reverse PTs occur in dif-
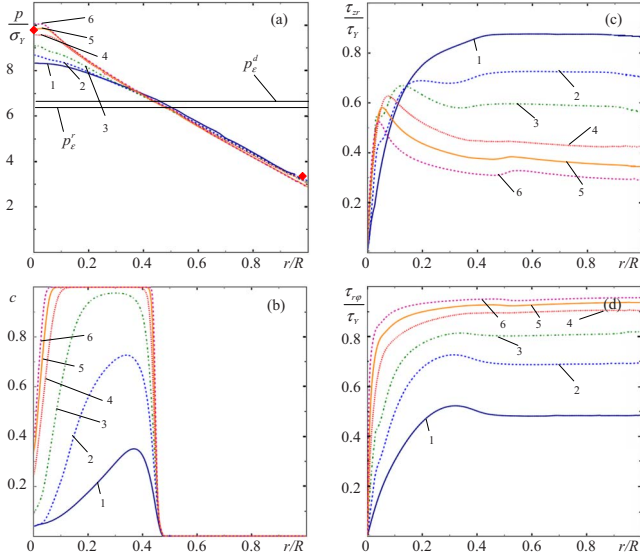
FIG. 3. (Color online) (a) Distributions of pressure p, (b) concentration of high-pressure phase c, (c) shear stress τ_{zr}, and (d) shear stress $\tau_{r\varphi}$ along the radius of the contact surface of a sample r for the case with $\sigma_{2y} = \sigma_{1y}$ for dimensionless applied axial force $F = 4.44$ and different values of angle of rotation φ. 1: $\varphi = 0.04$, 2: $\varphi = 0.14$, 3: $\varphi = 0.34$, 4: $\varphi = 0.78$, 5: $\varphi = 1.16$, and 6: $\varphi = 1.58$. Diamonds $\Diamond$ designate two points of straight line according to Eq. (2).

ferent regions of a sample. Observation of the high-pressure phase in the low-pressure region due to convective flow can lead to misinterpretation of experimental results. Since pressure distribution does not show any signature of PT, it is very difficult to determine kinetic parameters p_ε^d and p_ε^r from experiment.

B. Phase transformations to a stronger high-pressure phase

We will discuss the results of simulation of PT induced by torsion under fixed axial force $F = 4.44$ when $\sigma_{y2} = 5\sigma_{y1}$, see Figs. 4 and 5. Qualitatively, the character of evolution of distribution of accumulated plastic strain with growing rotation angle [Fig. 4(b)] is similar to the case with equal strength of the phases. However, due to strengthening of the material during the PT, reduction in the sample thickness is slightly lower (Fig. 14), and with the increase of the angle of rotation from $\varphi = 0.09$ to $\varphi = 1.30$, the maximum value of q grows from 12.2 to 88.3, i.e., to the values lower than for equal σ_y. At the same time, pressure (and all normal stresses) grow significantly in the transforming region where $p > p_\varepsilon^d$, despite the volume decrease due to PT. This is similar to the experimentally observed pressure self-multiplication effect for KCl and fullerene C_{60}.[6–9] The reduction in thickness due to torsion compensates the transformation-induced volume decrease and higher yield strength leads to an increase in radial friction stresses, and, consequently, to pressure growth. This result does not contradict the Le Chatelier principle of classical equilibrium thermodynamics because it is not applicable to nonhomogeneous, strain-induced PTs. This pressure increase during PT accelerates PT kinetics and serves as a positive mechanochemical feedback. A pressure

increase in the central part of the sample at constant axial force leads to a slight pressure decrease in the nontransformed part of the sample, which area is much larger than that for the transforming part. Pressure and all normal stresses grow almost linearly along the contact surface with different slopes in the nontransforming and transforming regions. A clear plateau (step) at the pressure distribution [Fig. 5(a)] in the region of diffuse interface between phases is formed, similar to that in experiments.[7–9] Pressure at a step slightly varies between p_ε^d and p_ε^r, and this result allows us to approximately identify these two key material parameters from experiments with the rotation of an anvil. Similar plateaus are observed in the distribution of normal stresses σ_{zz} and σ_{rr} (see Figs. S5a and S5b in Ref. 5). The character of the pressure contour lines [Fig. 4(c)] does not change with rotation and that pressure at the symmetry plane is always slightly lower than at the contact surface. The region without strain-induced PT (with magenta color) practically does not move during torsion, with the exception of the near contact region, where a plateau in pressure distribution is formed.

The distribution $c(r,z)$ [Fig. 4(a)] is qualitatively also similar to the case with $\sigma_{y1} = \sigma_{y2}$. One difference is that PT first completes at the contact surface. Radial plastic flow moves the high-pressure phase in the region with $p < p_\varepsilon^r$, where reverse PT starts. Finding in experiment a high-pressure phase at low pressure may lead to misinterpretation of experimental data and a claim of PT pressure below actual value, similar to the case with $\sigma_{y2} = \sigma_{y1}$.

Radial τ_{zr} and torsional $\tau_{r\varphi}$ shear stresses [Figs. 5(c) and 5(d)] along the contact surface in the nontransformed region are homogeneous; an increase in $\tau_{r\varphi}$ is accompanied by a decrease in τ_{zr} to keep $\tau = \sqrt{\tau_{r\phi}^2 + \tau_{zr}^2} = \tau_{y1}$, as in the previous case. In the transforming region, $\tau_{r\varphi}$ grows due to both an increase in rotation angle (as for the case with $\sigma_{y1} = \sigma_{y2}$) and an increase in the yield strength during the PT. These two factors change the radial τ_{zr} in opposite directions. For the initial rotation stage, τ_{zr} increases due to the increase in the yield strength. Then, PT is completed at the contact surface, the magnitude τ reaches the yield strength τ_{y2} and τ_{zr} decreases (excluding the small region near the sample center) due to the increase in $\tau_{r\varphi}$.

To summarize, the main features of the simulation for the case $\sigma_{y2} = 5\sigma_{y1}$ are: (1) reproduction of the pressure self-multiplication effect that was observed experimentally;[6–9] (2) reproduction of the plateau at the pressure (in fact, all normal stresses) distribution along the contact surface that was observed experimentally;[6–9] (3) this plateau corresponds to the diffuse interface between the phases; (4) pressure at the plateau varies between p_ε^d and p_ε^r and can be used to determine these important pressures from experiment. Thus, for KCl, $p_\varepsilon^d \simeq p_\varepsilon^r \simeq 1.8$ GPa, based on data in Ref. 7; and (5) radial plastic flow (however, less intense than for the case with $\sigma_{y2} = \sigma_{y1}$) moves the high-pressure phase in the region with $p < p_\varepsilon^r$, leading to reverse PT and possible misinterpretation of experimental data, similar to the case with $\sigma_{y2} = \sigma_{y1}$.

C. Phase transformations to a weaker high-pressure phase

Results for the case with $\sigma_{y2} = 0.2\sigma_{y1}$ are significantly different from both previous cases, see Figs. 6 and 7. The gen-
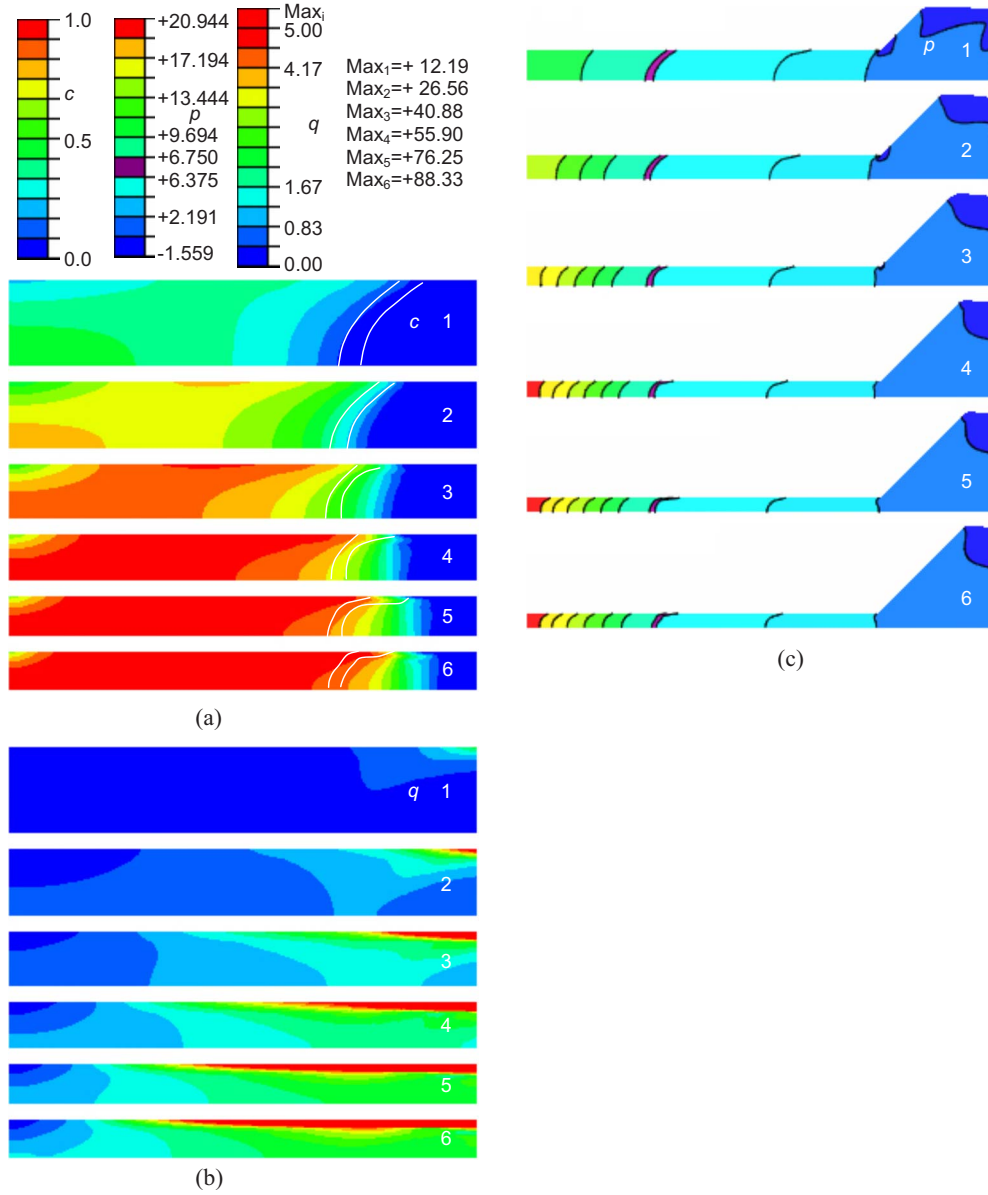
FIG. 4. (Color online) (a) Distributions of concentration of high-pressure phase c, (b) accumulated plastic strain q, and (c) pressure p for the case with $\sigma_{2y} = 5\sigma_{1y}$ for dimensionless applied axial force $F = 4.44$ and different values of angle of rotation φ. 1: $\varphi = 0.09$, 2: $\varphi = 0.38$, 3: $\varphi = 0.61$, 4: $\varphi = 0.94$, 5: $\varphi = 1.10$, and 6: $\varphi = 1.30$.

eral trend of evolution of all fields is governed by the softening of material during the PT, leading to material instability and strain and concentration localization in some regions. Instability leads to an irregular character of distribution of all fields. PT is not completed in the entire central part of the sample. Both plastic strain and concentration of high-pressure phase are localized in two regions: near the contact surface for $r/R > 0.36$ and near the symmetry plane for $r/R < 0.11$. In these regions, PT is completed at a very early stage of rotation $\varphi < 0.09$. The regions with complete PT are always separated, because the magenta region, in which strain-induced PT is impossible, lies between them. In fact, this region has quite complex, multiconnected geometry. After transformed material is moved by radial plastic flow in the region with $p < p_\varepsilon^r$, reverse PT occurs quite fast because plastic strain is concentrated in these weak regions.

Large plastic strain spreading across the entire sample thickness [Fig. 6(b), frame 4) is an evidence of convective flow of the weak partially or completely transformed regions.

In the nontransformed region, pressure and all normal stresses do not change appreciably during the torsion. Along the contact surface [Fig. 7(b)], PT mostly develops and completes in the growing ring. In this region, pressure evolves in an irregular way, exhibiting oscillations close to the value p_ε^d, which can be used to determine this parameter from the experiment. After the completion of the PT, pressure grows in this region. In the central region of a sample, pressure reduces at the initial stage of rotation, producing plateaus corresponding to p_ε^d, then to p_ε^r, and decreasing further causes reverse PT. Due to these results, it is difficult to extract information about p_ε^d and/or p_ε^r in this region. At further rotation, pressure increases in the central region, without essen-
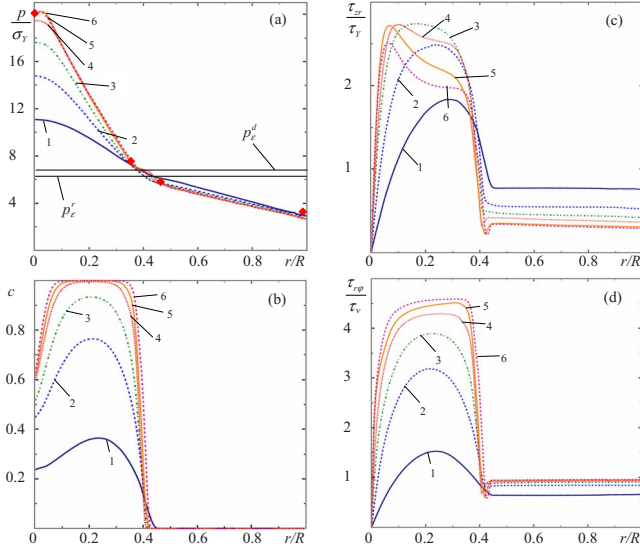
FIG. 5. (Color online) (a) Distributions of pressure p, (b) concentration of high-pressure phase c, (c) shear stress τ_{zr}, and (d) shear stress $\tau_{r\varphi}$ along the radius of the contact surface of a sample r for the case with $\sigma_{2y} = 5\sigma_{1y}$ for dimensionless applied axial force $F=4.44$ and different values of angle of rotation φ in a quarter of cross section of the sample. 1: $\varphi=0.09$, 2: $\varphi=0.38$, 3: $\varphi=0.61$, 4: $\varphi=0.94$, 5: $\varphi=1.10$, and 6: $\varphi=1.30$. Diamonds $\diamond$ designate two points of straight lines for $\sigma_y = \sigma_{y1}$ and $\sigma_y = \sigma_{y2}$ according to Eq. (2).

tial PT, due to low plastic strain. Since normal stresses almost do not vary in the peripheral part of the sample (which mostly contributes to the axial force) and vary only a little at the center, the curve of reduction in the sample thickness versus rotation angle is the same as for the constant yield strength (Fig. 14).

Shear stresses at the contact surface vary in a very heterogeneous and oscillatory way [see Figs. 7(c) and 7(d), and S3, c and d]. In the nontransformed part of a sample, these stresses are quasihomogeneous, $\tau_{r\varphi}$ increases, and τ_{zr} decreases to keep the magnitude of the friction shear stress vector $\tau = \tau_{y1}$ constant, similar to the previous cases. In the region of low-strength phase, both shear stresses are getting much lower to satisfy condition $\tau = \tau_{y2}$.

Summarizing, there is strong localization of plastic strain and concentration of the high-pressure phase, when it is significantly weaker than the low-pressure phase. This instability leads to the irregular character of all stress and concentration fields. It is not a numerical error, because such irregular pressure fields are observed experimentally for ZnSe (Fig. S9) Refs. 5 and 10) and CuI,[11] in contrast to the smooth pressure distribution for KCl (Refs. 7 and 8) and fullerene.[8,9] There are several plateaus in the pressure distribution, the pressure at which varies during torsion and PT; some of them are related to the characteristic pressures p_ε^d and/or p_ε^r for some rotation angles, and others are not. That is why it is very difficult to determine these parameters from experiments. Due to localized PT, the total amount of transformed material in the sample is smaller than for the two previous cases. The change in thickness versus rotation angle is the same as for the constant yield strength.

IV. COMPARISON OF PHASE TRANSFORMATIONS UNDER COMPRESSION AND TORSION AT CONSTANT FORCE

Comparisons of the fields and distribution curves along the contact surface after compression and after torsion for three yield-strength ratios are presented in Figs. 8–13. Torsion was performed at force $F=4.44$ and compression without torsion was performed at the same pressure at the sample center as it was for torsion. For all cases, PT starts at the center of the sample, where pressure first exceeds p_ε^d and where some strain localization occurs along the slip line. Another local maximum in c appears along the contact surface in the region with very large plastic strain. Note that strain-induced PTs occur for both loadings. Thus, the physics, thermodynamics, and kinetics are the same, with only the p-q paths at each point differing.

A. Comparison for equal yield strengths of phases

Compression was performed at forces $F=4.46$, 5.04, and 5.43, to be compared with the force $F=4.44$ for torsion. Torsion promotes the growth of the accumulated plastic strain q [Fig. 8(c)] in the sample (by a factor of 3–15), which in turn promotes the PT. Thus, with the increase in pressure at the center from 8.4 to 10.2 due to compression, the maximum value of q grows from 3.3 to 9.2. During torsion from $\varphi = 0.04$ to 1.57, the maximum value of q increases from 9.4 to 151.8. More important for PT is that during torsion q grows significantly not along the contact surface only but also in the interior of the sample.

For both regimes, almost linear growth of the pressure along the radius of the contact surface without any noticeable plateau in the area of phase interface is observed [Figs. 8(a) and 9(a)]. During torsion, the pressure slightly increases at the center and reduces at the periphery, without visible changing of the magenta region with $p_\varepsilon^d > p > p_\varepsilon^r$. Due to intense reduction in sample thickness, the high-pressure phase flows to the region with $p < p_\varepsilon^r$, and reverse PT occurs. In contrast, during compression pressure increases everywhere (due to an increase in applied force), and therefore the region where direct PT occurs expands. The reduction in thickness is less intense, and the high-pressure phase does not reach the region with $p < p_\varepsilon^r$; therefore, reverse PT never takes place.

Torsion drastically intensifies the PT [Figs. 8(b) and 9(b)] and leads to its completion in practically the entire region with $r/R \leq 0.48$ at $\varphi=1.57$. In contrast, under compression with the higher force $F=5.43$, maximum concentration of the high-pressure phase does not exceed 0.6, while PT is spread to $r/r \leq 0.65$. We have to increase force at least to 6.73, corresponding to a pressure at the center of 14.3, to obtain complete PT in some central region of a sample (see Figs. 2 and 4 in Ref. 1). This region is significantly smaller than the region with $p > p_\varepsilon^d$, in which PT completes near the contact surface only, because of much smaller plastic strain below the contact surface.

As was mentioned in Sec. III A, due to intense radial plastic flow, the lack of any PT signature in the pressure distribution, and the lack of correlation between the interface
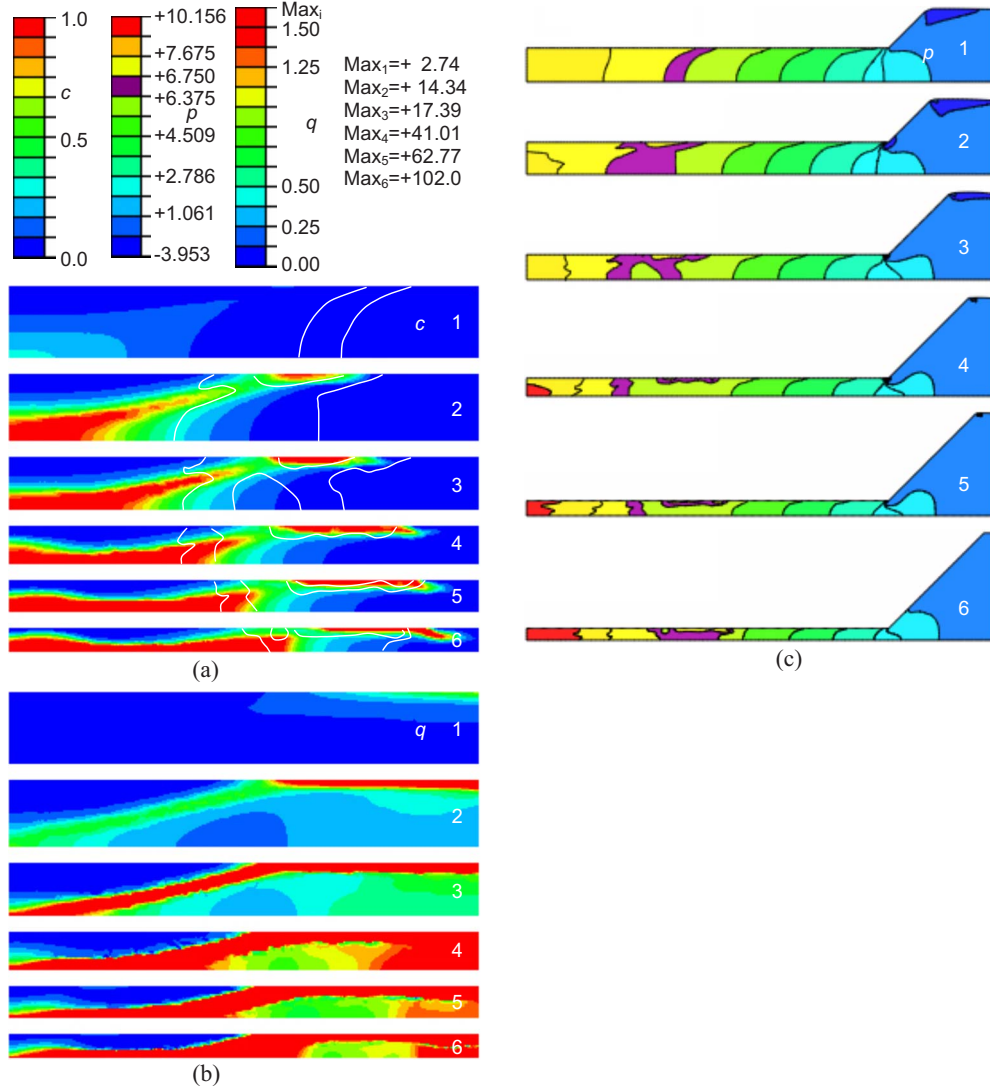
FIG. 6. (Color online) (a) Distributions of concentration of high-pressure phase c, (b) accumulated plastic strain q, and (c) pressure p for the case with $\sigma_{2y}=0.2\sigma_{1y}$ for dimensionless applied axial force $F=4.44$ (except 1) and different values of angle of rotation φ. 1: $F=4.30$, $\varphi=0.0$, 2: $\varphi=0.09$, 3: $\varphi=0.20$, 4: $\varphi=0.64$, 5: $\varphi=0.84$, and 6: $\varphi=1.40$.

between phases and the characteristic pressures p_d^r and p_ε^r, it is very difficult to determine these parameters from experiment for this case. It is also difficult for the compression regime. However, because of smaller reduction in sample thickness and less-developed radial flow, for any compression stage, pressure at the contact surface at the point where PT starts corresponds to the characteristic pressure p_d^ε. This correspondence is more robust for large forces, when PT is complete (see Figs. 2 and 4 in Ref. 1). This may allow us to determine p_d^ε in experiment. However, we do not see any way to find p_r^ε for this case experimentally.

Summarizing, torsion significantly intensifies PT and allows us to complete PT (at the same contact pressure on the symmetry axis) at significantly lower axial force than for compression. The transforming region, however, is smaller than for compression, due to both a smaller region with $p>p_\varepsilon^d$ and a larger reduction in sample thickness. When comparing with results for compression at the same axial force (Fig. 2 in Ref. 1), torsion allows us to complete PT (Fig. 9)

almost in the entire region with $p>p_\varepsilon^d$. Pressure at the center of a sample is significantly higher than p_ε^d but it grows slightly only during torsion.

B. Comparison for phase transformation to a stronger high-pressure phase

Torsion increases the Odqvist parameter q in the sample by a factor of 2–5 in comparison with compression [Fig. 10(c)]. With an increase in pressure (without torsion) from 12.4 to 20.1, q_{max} grows from 7.7 to 16.5. With a similar increase in pressure due to the torsion q_{max} increases from 18.3 to 76.3. Torsion also leads to a significant increase in q in the interior of the sample, which allows us to complete PT in almost the entire region where $p>p_\varepsilon^d$. During the torsion, pressure strongly increases [Figs. 10(a) and 11(a)] in the transforming region only (due to an increase in the yield strength) and slightly decreases in the nontransforming area (to keep the same axial force). The transforming region prac-
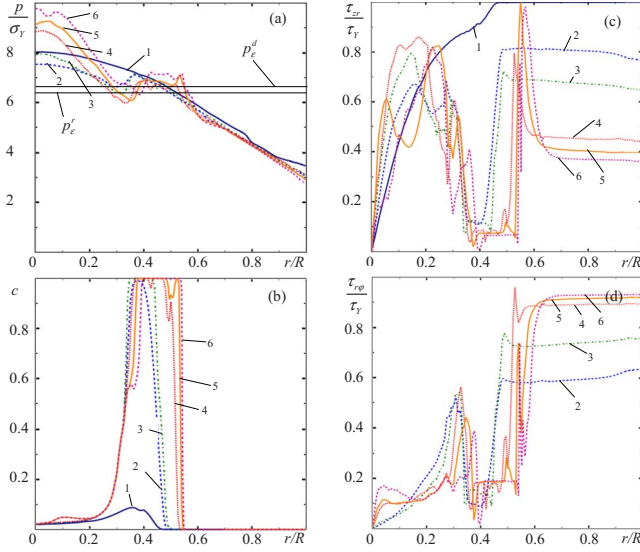
FIG. 7. (Color online) (a) Distributions of pressure p, (b) concentration of high-pressure phase c, (c) shear stress τ_{zr}, and (d) shear stress $\tau_{r\varphi}$ along the radius of the contact surface of a sample r for the case with $\sigma_{2y} = 0.2\sigma_{1y}$ for dimensionless applied axial force $F = 4.44$ (except 1) and different values of angle of rotation φ. 1: $F = 4.30$, $\varphi = 0.0$, 2: $\varphi = 0.09$, 3: $\varphi = 0.20$, 4: $\varphi = 0.64$, 5: $\varphi = 0.84$, and 6: $\varphi = 1.40$.

tically does not change its radius during rotation of an anvil. For PT under compression without torsion, pressure grows in an entire sample (which requires a significant increase in the axial force), and the transforming region spreads in the radial direction. Therefore, the torsion on the one hand promotes PT in the high-pressure region of the sample, and on the other hand it limits the region of the sample, where PT occurs. Without torsion, a high-pressure phase may propagate throughout the whole sample. With a noticeable torsion, plateau is observed in the area of diffuse phase interface, which is located between p_{ε}^{d} and p_{ε}^{r}. This allows us to identify these two key material parameters in experiment. In experiments a plateau is observed during compression as well[7–9] and pressure at the plateaus is reduced after torsion. However, we did not observe plateaus under compression for $\sigma_{y2} \geq \sigma_{y1}$, which may be because of relatively slow kinetics or some missing physics in the model.

PT spreads in the radial direction faster without torsion, than with torsion [Figs. 10(b) and 11(b)]. However, PT progresses faster along the height of a sample with torsion. Also, under compression up to the highest force under consideration, PT does not complete in any region. In contrast, torsion significantly intensifies PT in the region where $p > p_{\varepsilon}^{d}$ and leads to complete PT there. At maximum pressure $p = 20.1$, PT occurs (although it is not yet complete) in the region $r/R < 0.68$ at $F = 7.21$ under compression and is complete PT in the region $r/R < 0.44$ at $F = 4.44$, and $\varphi = 1.11$ for torsion. During torsion, the high-pressure phase flows to the region where $p < p_{\varepsilon}^{r}$ and reverse PT occurs. This corresponds to experimental findings;[7] see the position of the arrow indicating a visible interface in Fig. S8 (Ref. [5]) before and after rotation. For compression, radial flow is less intense and pressure grows faster, and the high-pressure phase does not

reach the region where $p < p_{\varepsilon}^{r}$. It is visible in Fig. 10, a that the torsion leads to much more intense reduction in the sample thickness. With pressure at the center $p = 20.1$ the difference in the axial deformation is about 40%. From Fig. 11(b) we conclude that torsion indeed leads to a sharper phase interface, which corresponds to experiments on KCl.[7]

Summarizing, torsion significantly intensifies PT and allows us to complete PT at the same contact pressure at the center under significantly lower axial force than for compression, similar to the case with $\sigma_{y2} = \sigma_{y1}$. The transforming region, is also smaller than for compression, both due to a smaller region with $p > p_{\varepsilon}^{d}$ and reduction in the sample thickness during the torsion. In comparison with compression at the same axial force (Fig. 6 in Ref. [1]), torsion (Fig. 5) induces complete PT almost in the entire region with $p > p_{\varepsilon}^{d}$. Pressure at the center of a sample for complete PT is drastically larger than p_{ε}^{d} and it drastically grows during torsion at constant force (the pressure self-multiplication effect).

C. Comparison for phase transformations to a weaker high-pressure phase

Here, the results for the PT under compression by increasing force $F = 5.07$, 5.42, and 6.11, and under torsion under the load $F = 4.44$ are compared for the case $\sigma_{y2} = 0.2\sigma_{y1}$. For all cases in Fig. 12(c), strong strain localization near the contact surface of the sample and along the line connecting the center of a sample with the contact surface is observed. Accumulated plastic strain for the torsion has similar contour lines to the ones without torsion, only with higher values, by a factor of 1.5–2. For example, with an increase in pressure at the center from 7.95 to 8.80 (without torsion), q_{max} grows from 11.7 to 22.1. With a similar increase in pressure due to torsion, q_{max} increases from 17.4 to 41.

An irregular pressure distribution [see Figs. 12(a) and 13(a)] is observed in both cases. Under torsion, pressure at the contact surface changes slightly for $\varphi \leq 0.32$ and grows at the center for $\varphi = 0.64$. In this region, pressure is lower than p_{ε}^{d} and even p_{ε}^{r}, which arrests direct PT and causes the reverse PT in the transformed region. At the plateau region, pressure initially exceeded p_{ε}^{d}, which in combination with large plastic strain caused complete PT [see Fig. 13(b)]. For large rotation, pressure drops in this region, but it grows slightly for larger r, which leads to expansion of the transformed region. At the external part of the sample, pressure does not change during rotation. In comparison, under compression, pressure at the contact surface grows everywhere, increasing the transforming region. There is a plateau under compression in the region where PT is completed, which is above the plateau after torsion–i.e., as in experiments for PT CuI.[11] It is significantly above the value of p_{ε}^{d} and is not related to any characteristic pressure in the kinetic equation. Thus, while the experimentalists used pressure at this plateau as "PT pressure" (see Refs. [10] and [11]), its interpretation does not have any physical sense at the moment. For torsion, pressure oscillates near the values p_{ε}^{d} and p_{ε}^{r}, which can be used for experimental determination of these parameters. In Fig. 13(a), there are several steps on the $p(r)$ curve corresponding to p_{ε}^{d} and p_{ε}^{r}.
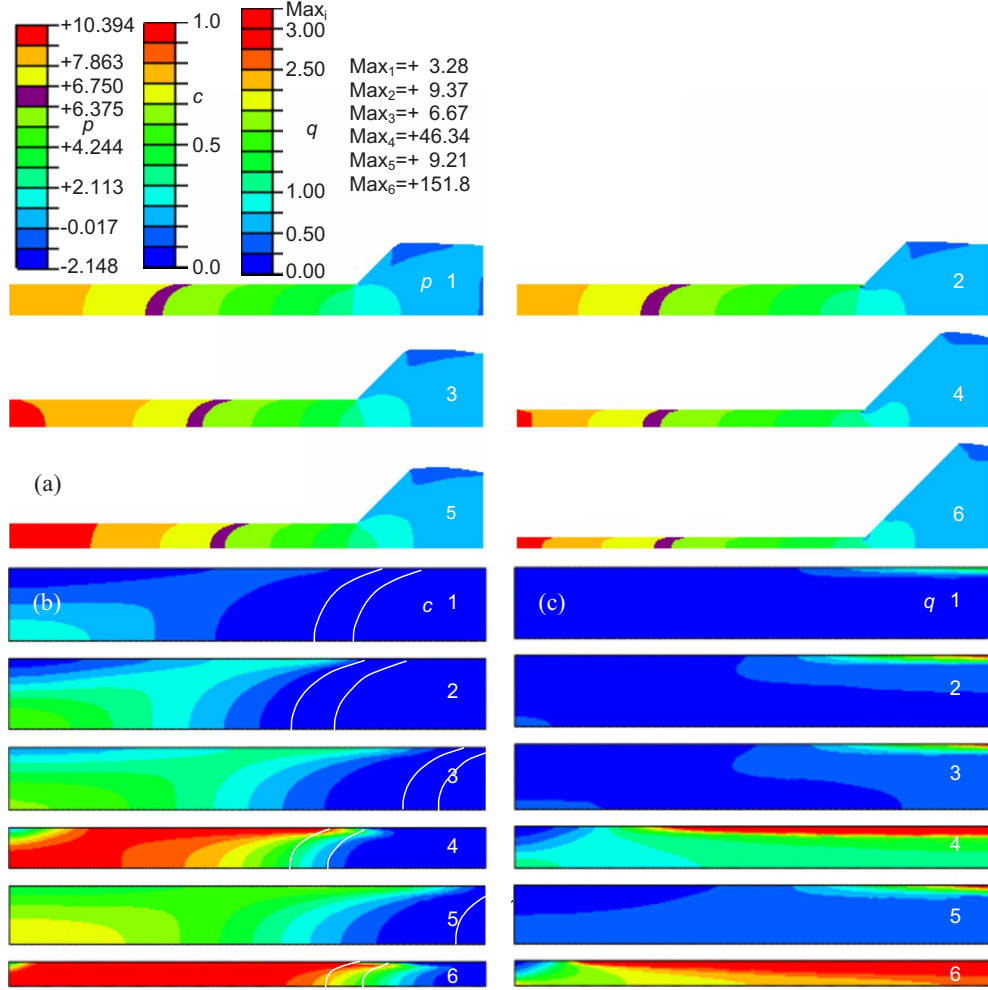
FIG. 8. (Color online) (a) Comparison of distributions of pressure p, (b) concentration of high-pressure phase c, (c) accumulated plastic strain q for compression (1, 3, and 5) and torsion (2, 4, and 6) for $\sigma_{y2} = \sigma_{y1}$. The pressure at the contact surface at $r=0$ after pure compression and torsion is the same and equal to 8.40 (1 and 2), 9.40 (3 and 4), and 10.2 (5 and 6). The dimensionless force F is 4.46 (1), 5.04 (3), 5.43 (5), and 4.44 (2, 4, and 6). Rotation angle φ is 0.04 (2), 0.60 (4), and 1.57 (6).

Under compression, pressure grows in the entire volume, shifting the magenta "nontransformation" region to larger r. For torsion, the nontransformation region is multiconnected. The transforming region with $p > p_\varepsilon^d$ is located at the center of the sample and as a small island near the contact surface. Compression leads to the complete PT at the contact surface in the ring, which expands [Figs. 12(b) and 13(b)]. In the central region, PT just started due to small plastic strains. Under the largest force, $F=6.11$, there is an additional increment of concentration at the center, still not exceeding 0.3. Under torsion, the complete PT occurs in a much narrower ring, which slightly shifts to larger r for $\varphi=0.32$ (i.e., both direct and reverse PTs occur simultaneously at different sides of the ring, due to pressure redistribution) and then expands toward larger r for $\varphi=0.64$. Still, the completely transformed ring at the largest $\varphi=0.64$ is smaller than that for the smallest force, $F=5.07$, under compression. Phase interfaces for all cases are quite sharp due to drastic localization of plastic strain. In the volume, the regions with fully transformed material are larger for compression than for torsion. For compression, it is a single connected region localized along the shear band that grows due to pressure growth. For torsion, this is a region at the center of a sample and a thin ring near the contact surface, separated by a no-transformation region and a region with $p < p_\varepsilon^r$, where reverse PT occurs. Due to a larger reduction in thickness under torsion, the total amount of transformed phase is significantly larger for compression, which may be important for a obtaining strong signal in an x-ray experiment.

Summarizing, for the PT to the weaker phase, pressure at the plateau (which corresponds to the completely transformed region near the contact surface) reduces during the torsion, both in the above calculations and in experiments,[10,11] which was interpreted by the experimentalist as a reduction in PT pressure due to plastic shear. However, pressure at the plateau is higher than p_ε^d and does not correspond to any characteristic pressure, so its reduction during rotation to the values p_ε^d and p_ε^r, does not prove that PT pressure reduces. Recall that the notion of PT pressure for strain-induced PT is not defined because it can occur at any pressure above p_ε^r. On the contrary, our calculations shows that torsion in this case does not promote strain-induced PT,
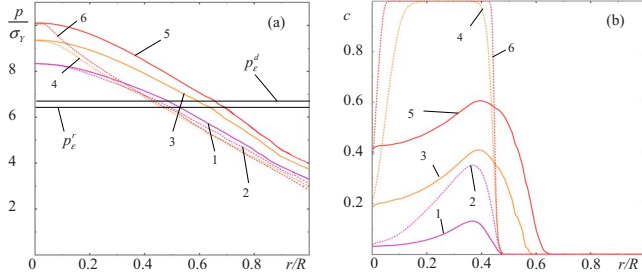
FIG. 9. (Color online) (a) Comparison of distributions of pressure p and (b) concentration of high-pressure phase c for compression (1, 3, and 5) and torsion (2, 4, and 6) for $\sigma_{y2}=\sigma_{y1}$. The pressure at the contact surface at $r=0$ after pure compression and torsion is the same and equal to 8.40 (1 and 2), 9.40 (3 and 4), and 10.2 (5 and 6). Dimensionless applied axial force F is 4.46 (1), 5.04 (3), 5.43 (5), and 4.44 (2, 4, 6). Rotation angle φ is 0.04 (2), 0.60 (4), and 1.57 (6).

because at the same maximum pressure in the center of a sample, it leads to complete PT in a smaller region, due to both pressure redistribution and reduction in the sample thickness. However, axial force in these calculations is smaller for the case with torsion.

V. COMPARISON WITH A SIMPLIFIED MODEL

In Refs. 12 and 13, the only analytical study of strain-induced PTs is performed. The main equation for analysis of experiments under compression and compression with torsion and for analytical treatment is the simplified equilibrium equation[12,13]

$$dp/dr = -2\tau_{rz}(h/2)/h, \qquad (2)$$

where $\tau_{rz}(h/2)$ is the radial friction stress at the contact. The theory in Refs. 12 and 13 considers a cylindrical sample only ($r \leq R$), i.e., part of the force and torque related to the external part of a sample $r > R$ with their evolution being neglected. The condition $\tau = \tau_y$ is assumed along the entire contact surface and it is assumed that the angle of inclination of the vector of friction stress τ to the radius is independent of r. Equation (1) is also utilized. For compression, $\tau_{rz}(h/2) = \tau_y$. For torsion under constant load, Eq. (2) was reduced in Refs. 12 and 13 to

$$\frac{dp}{dr} = \frac{2\tau_y}{h_0}, \qquad (3)$$

where h_0 is the sample thickness at the beginning of rotation. Since $h_0 = \text{const}$, Eq. (3) coincides with the equilibrium equa-
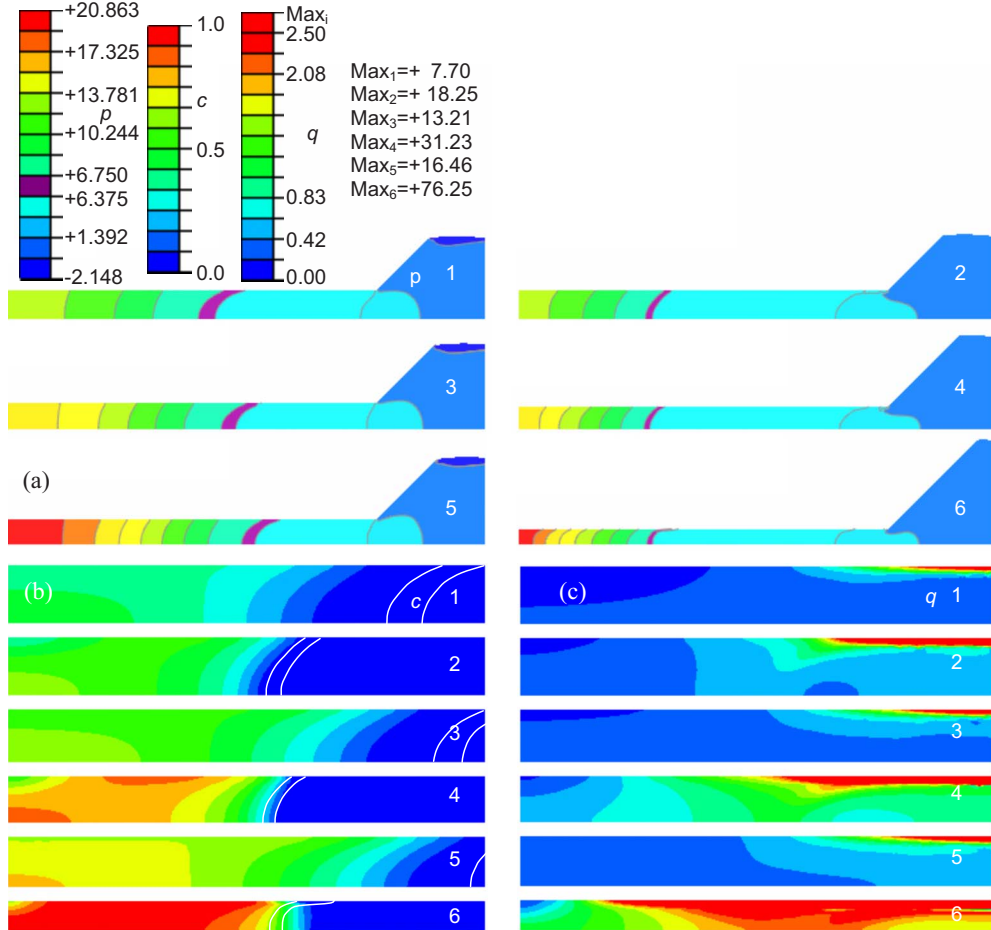

FIG. 10. (Color online) (a) Comparison of distributions of pressure p, (b) concentration of high-pressure phase c, (c) accumulated plastic strain q for compression (1, 3, and 5) and torsion (2, 4, and 6) for $\sigma_{y2}=5\sigma_{y1}$. The pressure at the contact surface at $r=0$ after pure compression and torsion is the same and equal to 12.4 (1 and 2), 16.2 (3 and 4), and 20.1 (5 and 6). Dimensionless force F is 5.47 (1), 6.26 (3), 7.21 (5), and 4.44 (2, 4, and 6). Rotation angle φ is 0.20 (2), 0.52 (4), and 1.11 (6).
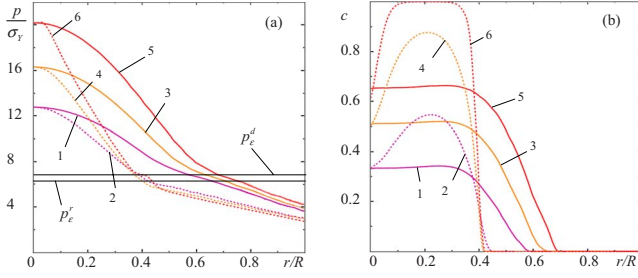
FIG. 11. (Color online) (a) Comparison of distributions of pressure p and (b) concentration of high-pressure phase c for compression (1, 3, and 5) and torsion (2, 4, and 6) for $\sigma_{y2}=5\sigma_{y1}$. The pressure at the contact surface at $r=0$ after pure compression and torsion is the same and equal to 12.4 (1 and 2), 16.2 (3 and 4), and 20.1 (5 and 6). Dimensionless applied axial force F is equal to 5.47 (1), 6.26 (3), 7.21 (5), and 4.44 (2, 4, and 6). Rotation angle φ is equal to 0.20 (2), 0.52 (4), and 1.11 (6).

tion for compression under the same force F. Since the yield strength does not change in the nontransformed (i.e., $\tau_y = \tau_{y1}$) and fully transformed (i.e., $\tau_y = \tau_{y2}$) parts, the solution to Eq. (3) represents the piecewise linear pressure distribution. Also, for $\sigma_{y1}=\sigma_{y2}$ the pressure distribution is independent of the rotation of an anvil. It is clear from Fig. 3(a) that

for $\sigma_{y1}=\sigma_{y2}$, pressure distribution is indeed independent of φ in the region where $\tau=\tau_y$. Also, Eq. (3) gives practically the same slope as the FEM solution: (a) for $\sigma_{y1}=\sigma_{y2}$, (b) in nontransformed region $\sigma_{y2}=0.2\sigma_{y1}$ and $\sigma_{y1}=\sigma_{y2}$, and (c) in the fully transformed regions for $\sigma_{y2}=5\sigma_{y1}$ [see Figs. 3(a), 5(a), and 7(a)]. Note that in *experiments* for NaCl in Ref. 7 and for stainless steel in Ref. 8, the independence of the pressure distribution of φ was found for the case without PT. However, there is no, any, correspondence between analytical and FEM solutions in the transforming region for $\sigma_{y2}=0.2\sigma_{y1}$ [Fig. 7(a)], which implies that Eq. (2) *is not applicable for the case with strong plastic strain and concentration localization*. In particular, it was expected that pressure reduces at the center due to reduction in the yield strength but it starts to grow at some torsion stage. Equation (2) implies that zero pressure gradient at the plateau of the pressure distribution corresponds to $\tau_{rz}(h/2)=0$, which does not correspond to our FEM results [see Figs. 5(a) and 7(a)]. This means that Eq. (2) *is not valid in the regions with a large gradient of concentration and, consequently, plastic properties of phases.*

There were several attempts to explain zero pressure gradient based on Eq. (2). Thus, it was assumed in Ref. 14 that $\sigma_y=0$ in the plateau region during the PT. However, this contradicts numerous stress-strain curves for transformation-
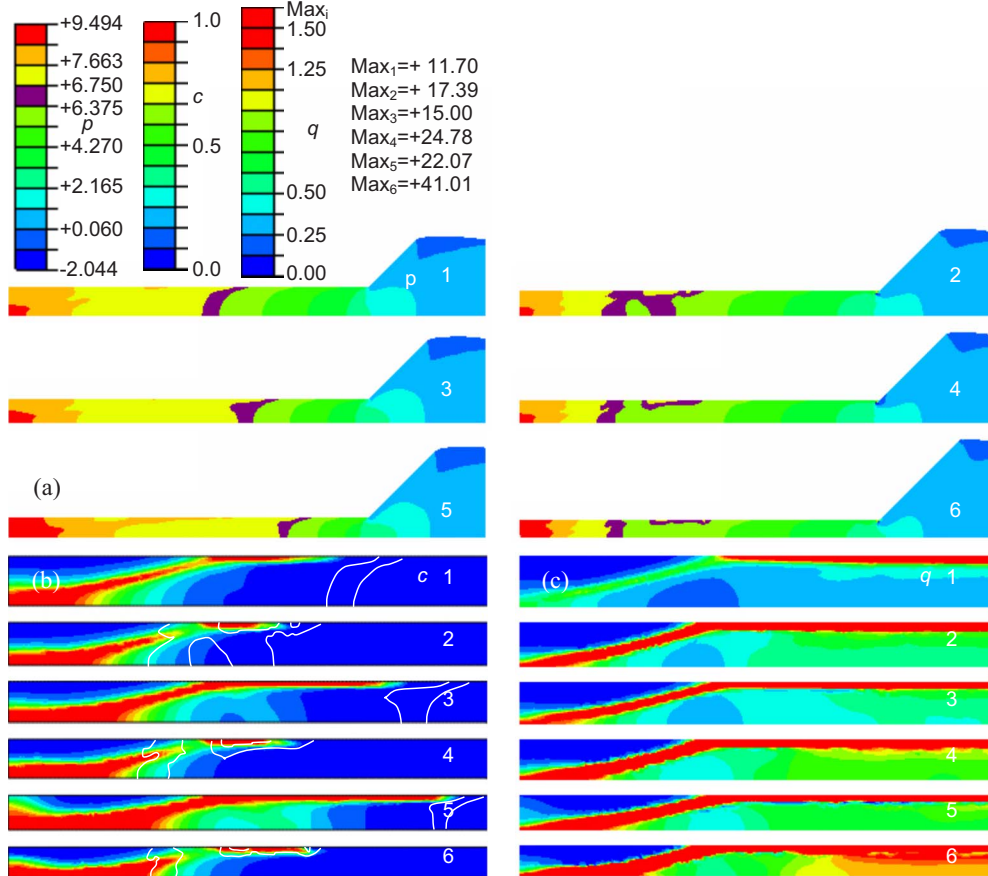

FIG. 12. (Color online) (a) Comparison of distributions of pressure p, (b) concentration of high-pressure phase c, (c) accumulated plastic strain q for compression (1, 3, and 5) and torsion (2, 4, and 6) for $\sigma_{y2}=0.2\sigma_{y1}$. The pressure at the contact surface at $r=0$ after pure compression and torsion is the same and equal to 7.95 (1 and 2), 8.10 (3 and 4), and 8.80 (5 and 6). Dimensionless force F is 5.07 (1), 5.42 (3), 6.11 (5), and 4.44 (2, 4, and 6). Rotation angle φ is 0.20 (2), 0.32 (4), and 0.64 (6).
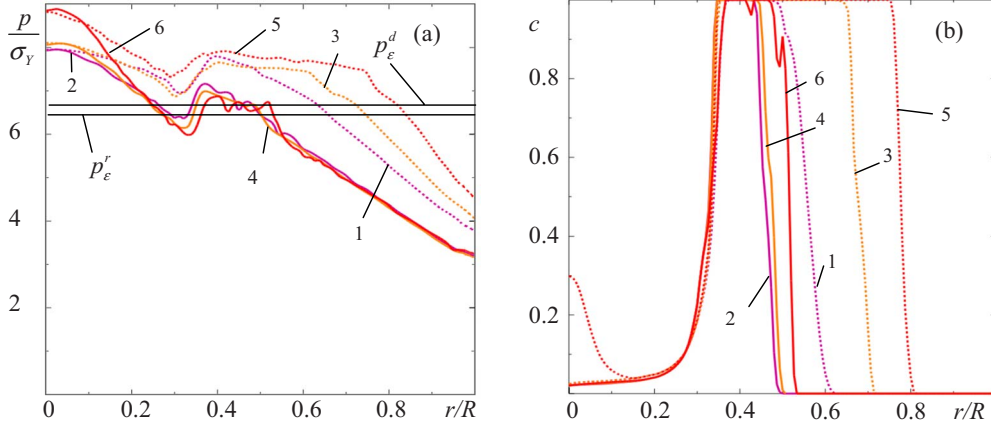
FIG. 13. (Color online) (a) Comparison of distributions of pressure p and (b) concentration of high-pressure phase c for compression (1, 3, and 5) and torsion (2, 4, and 6) for $\sigma_{y2}=0.2\sigma_{y1}$. The pressure at the contact surface at $r=0$ after pure compression and torsion is the same and equal to 7.95 (1 and 2), 8.10 (3 and 4), and 8.80 (5 and 6). Dimensionless applied axial force F is equal to 5.07 (1), 5.42 (3), 6.11 (5), and 4.44 (2, 4, and 6). Rotation angle φ is equal to 0.20 (2), 0.32 (4), and 0.64 (6).

induced plasticity (TRIP) steels during strain-induced PT.[15] Another assumption leading to $\tau_{rz}(h/2)=0$ was that the radial velocity at diffuse phase interface is zero due to the volume decrease during PT, which is not supported by our study. Also, an analytical model[12,13] demonstrates the possibility of reduction in $\tau_{rz}(h/2)=0$ during torsion up to zero due to TRIP. Should we include TRIP in our model, it may indeed lead to relaxation of shear stresses and to the appearance of a plateau in cases, in which we did not observe it.

The combination of Eqs. (24) and (25) from Ref. 13 leads to the following equation connecting the angle of rotation of an anvil and reduction in thickness during torsion,

$$\varphi = \frac{1+0.204m}{0.204m}\left(\sqrt{\frac{h_0^2}{h^2}-1}-\arccos\frac{h}{h_0}\right), \qquad (4)$$

where $m=R/H_0$ and PTs were neglected. Superposing this plot (for $m=5$) on the results of FEM simulation (Fig. 14), we find that it significantly higher. At the same time, it describes well FEM results without PTs.[3] It is not surprising because Eq. (4) does not take into account volumetric transformation strain equal to 0.1. However, deviation is larger than can be expected based on this strain. That means that volume change induces additional plastic flow called TRIP.

VI. COMPARISON WITH AND INTERPRETATION OF EXPERIMENTS

Below, the cases with qualitative correspondence between our simulations and experiments are presented. Since we used generic properties in our model and aimed to obtain results valid for a broad class of materials, rather than properties for specific materials (which are unknown), quantitative comparison is impossible.

(a) Experimentally observed plateaus in the pressure-distribution curve have been reproduced in our calculation. For $\sigma_{y2}=5\sigma_{y1}$, the plateau under torsion corresponds to the diffuse interface, as it was observed in experiments for KCl and fullerene C_{60}.[7–9] However, we were unable to reproduce the same steps for compression. It may appear for a different

choice of kinetic parameters; otherwise, some physics (for example, TRIP) is missing in the model. For $\sigma_{y2}=0.2\sigma_{y1}$, we succeeded in reproducing the steps both for compression and torsion, which were observed in experiments for ZnSe (Fig. S9) (Refs. 5 and 10) and CuI.[11]

(b) The irregular pressure distribution at the contact surface obtained for $\sigma_{y2}=0.2\sigma_{y1}$ corresponds to experiments for ZnSe (Fig. S9) (Refs. 5 and 10) and CuI.[11] The smooth pressure distribution obtained for $\sigma_{y2}=5\sigma_{y1}$ agrees with results for KCl (Ref. 7) and fullerene C_{60}.[8,9]

We should mention the smooth pressure plots for PT from the semiconducting phase III to the weaker metallic phase II in Ge and Si.[16,17] There are multiple PTs in these systems, including PTs from semiconducting phase I to the probably stronger, high-pressure semiconducting phase III (see our model in Ref. 18), which may lead to a smooth curve.

(c) Torsion leads to a sharper phase interface, which corresponds to experiments on KCl.[7] (d) A reduction in sample thickness during torsion under constant load is observed in Refs. 6 and 8.

(e) A slight increase in contact pressure at the center of a sample during PT in ZnSe (Fig. S9) (Refs. 5 and 10) under
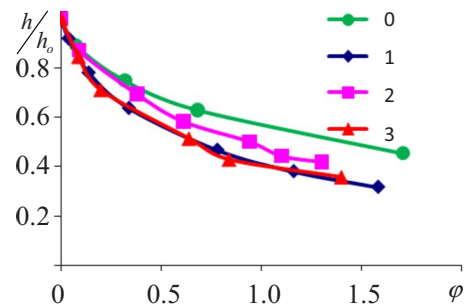

FIG. 14. (Color online) Change in relative thickness h/h_o of the sample vs angle of rotation φ for (1) $\sigma_{y2}=\sigma_{y1}$, (2) $\sigma_{y2}=5\sigma_{y1}$, and (3) $\sigma_{y2}=0.2\sigma_{y1}$, and (0) according to Eq. (4).

torsion supports our results for $\sigma_{y2} < \sigma_{y1}$ and large rotation (while it contradicts a simplified model). Pressure at the center of sample reduces during torsion of Si,[16] which corresponds to our results for $\sigma_{y2} < \sigma_{y1}$ and small rotation and may also be caused by a pressure increase at the periphery due to PT I→III. The reduction in pressure for PT in CuI (Ref. 11) cannot be compared with the current work because of the use of a gasket.

(f) During torsion, high-pressure phase flows to the region where $p < p_\varepsilon^r$ and reverse PT occurs, which is confirmed by experiment for KCl in Ref. 7 [Fig. S8 (Ref. 5)]. (g) In Ref. 19, PT from strong semiconducting Si I to weaker metallic Si II under compression in diamond anvils was found in a thin contact layer only but not in the bulk, which agrees with our simulation in Fig. 12(a). This coincidence also confirms the possibility of strain-induced (rather than pressure-induced) PT under compression without torsion.[1]

(h) For the case with increasing yield strength, during torsion the pressure grows significantly in the transforming region. Such a pressure growth despite the volume decrease due to PT does not contradict to the Le Chatelier principle because the thermodynamics of heterogeneous strain-induced PTs differs significantly from classical thermodynamics.[12,13] This result corresponds to the experimentally observed pressure self-multiplication effect.[6–9] The decrease in sample thickness during torsion compensates for the transformation-induced volume decrease and higher yield strength leads to the increase in pressure.

The following results have important consequence for interpretation of experiments. (a) The essential heterogeneity in concentration of the high-pressure phase (due to localization of plastic strain and strong radial heterogeneity in pressure) causes a significant problem in quantitative characterization of strain-induced PTs. There are two main experimental approaches to measure the concentration of a high-pressure phase in local points.[6,19–22] X-ray diffraction allows us to measure the concentration of the high-pressure phase averaged over the thickness of a sample. In contrast, the Raman method gives concentration averaged over the thin layer near the sample contact surface. Consequently, different measurement techniques will give different PT kinetics. This indeed was observed in experiments in Ref. 19, where PT from Si I to Si II under compression in diamond anvils was confirmed by the Raman method in a thin contact layer while PT did not occur in the bulk.

(b) The reduction in sample thickness during torsion leads to intense radial flow of the high-pressure phase to the low-pressure region, where the reverse strain-induced PT occurs. Thus, in experiment, the high-pressure phase may be found at a low pressure, at which it cannot be obtained due to PT. This may lead to incorrect numerical data for PT pressure and to overestimation of the effect of plastic deformation on PTs in general.

(c) The total amount of high-pressure phase and the amount of high-pressure phase for each r, is significantly larger for compression than for torsion, due to a smaller reduction in thickness. This may be important for obtaining a strong signal in x-ray experiments.

(d) Equation (2) was routinely used for interpretation of data on pressure distribution. We found that in combination with the analytical model[12,13] it reproduces well the $p(r)$ distribution in the nontransforming zone for all combinations of the yield strengths; it describes well $p(r)$ for $\sigma_{y2} = \sigma_{y1}$ and its independence of the rotation angle; it also describes $p(r)$ in the completely transformed region for $\sigma_{y2} = 5\sigma_{y1}$. However, this model, and, in particular, Eq. (2), are not applicable for the case with $\sigma_{y2} = 0.2\sigma_{y1}$ and at the plateau of the pressure distribution for $\sigma_{y2} = 5\sigma_{y1}$. In both cases, due to large gradients of concentration of the high-pressure phase, a large gradient of the yield strength makes Eq. (2) inapplicable. This is a very important result because Eq. (2) leads to wrong intuition and formulation of a wrong problem on why condition $\tau_{rz}(h/2) = 0$ is held in the diffuse interface region. We found that $\tau_{rz}(h/2) \neq 0$ in this region while $dp/dr = 0$.

(e) The value of pressure at the plateau (step) of the experimental pressure distribution is currently used as the PT pressure, without exact understanding of what it means. In particular, in Ref. 7 it was identified as phase-equilibrium pressure, with the following arguments. First, a zero pressure gradient corresponds according to Eq. (2) to zero shear stress, i.e., to a hydrostatic condition. Second, plastic shear decreases plastic hysteresis, and since in Ref. 7 the pressure at the step was the same for direct and reverse PT, then pressure at the step is the phase-equilibrium pressure. The inconsistency of this consideration is discussed in Refs. 12 and 13 and is related to the fundamental difference between pressure-induced and strain-induced PTs. Strain-induced PT cannot be characterized by a specific pressure because it can occur at any pressure above p_ε^d. Ideally, it should be characterized by the kinetic relationship $c = f(p,q,c)$. Based on our simulation and available experimental methods (Raman and x ray) for determination of the concentration of the high-pressure phase, it is very difficult to do this due to heterogeneity in concentration, plastic strain, and pressure distribution and their variation during the loading increment. It may be much easier to determine kinetics from the experiments, when the sample is placed in a gasket with geometric parameters that result in quasihomogeneous pressure and concentration distributions along the radius with small variation during torsion.[6] An FEM study of this problem will be performed in the future to find the heterogeneity along the z direction and possibility to extract kinetic data from coupled experiments and simulations. Yet, we can consider the more modest problem of interpretation of values of pressure at the steps and determination of characteristic p_ε^d and p_ε^r in the kinetic equation. Our simulations show that for $\sigma_{y2} > \sigma_{y1}$ and under torsion, the pressure at the steps varies between p_ε^d and p_ε^r, and these parameters can be approximately determined from experiment. For more precise conclusion, our simulations will be repeated in the future for a larger difference between p_ε^d and p_ε^r and for $p_\varepsilon^d < p_\varepsilon^r$. Thus, based on data in Ref. 7, we can conclude that for KCl $p_\varepsilon^d \simeq p_\varepsilon^r \simeq 1.8$ GPa.

For $\sigma_{y2} = 0.2\sigma_{y1}$, the situation is much more sophisticated. A large plateau and small steps exist under both compression and torsion, similar to experiments.[10,11] A plateau under torsion corresponds to p_ε^d when PT is completed at the contact surface. Further rotation leads to a pressure increase at the plateau, which is not related to PT. Small steps evolve, and the pressure at them varies between p_ε^d and p_ε^r, decreasing below p_ε^r at further rotation. Thus, one may be able to deter-

mine p_ε^d and p_ε^r from experiment at the initial stage of rotation but it is not simple to determine at which rotation angle this stage ends. Under compression, a plateau appears when PT is completed in a ring at the contact surface and it is above the plateau after torsion, again similar to experiments for ZnSe (Fig. S9) (Refs. 5 and 10) and CuI.[11] Since pressure at the plateau is above p_ε^d, it is determined by the mechanics of plastic flow coupled with PT rather than by PT-related characteristics. In compression experiment for $\sigma_{y2} > \sigma_{y1}$, the plateau is also above the plateau after torsion,[7–9] i.e., above p_ε^d, which means that it also is not connected directly to PT-related characteristics.

We conclude that for torsion and $\sigma_{y2} > \sigma_{y1}$, the pressure at plateaus varies between p_ε^d and p_ε^r and can be used for experimental determination of these parameters. For torsion and $\sigma_{y2} < \sigma_{y1}$, the steps and plateau correspond to p_ε^d and p_ε^r, but it is not easy to distinguish them from steps and plateaus that are not PT related. For compression for any σ_y, pressure at the steps does not correspond to any PT-related parameter.

(f) Usually, the conclusion that plastic strain reduces the PT pressure comes from a reduction in pressure at plateaus during torsion. Since the concept of the PT pressure is not well defined for strain-induced PTs (which can occur at any pressure above p_ε^d) and pressure at compression is not directly related to characteristic PT pressure, this statement, while generally correct, does not follow from such an experiment. On the other hand, the possibility of strain-induced PT near the plateau region at pressure as low as $p = p_\varepsilon^d$, does prove the plastic strain-induced reduction in pressure and allows us to quantify it.

VII. CONCLUDING REMARKS

In this two-part paper, a 3D model for strain-induced PTs is developed, a computational procedure for the solution of a corresponding boundary-value problem is described, and FEM simulations of PTs under compression and torsion at fixed axial force in rotational anvil cell are performed. For all cases under study under compression in Ref. 1 and torsion here: (a) PT starts at the center of a sample, where the condition $p > p_\varepsilon^d$ is first met and where there is some strain localization; (b) another local maximum in concentration c was found along the contact surface in the region with intense localized plastic flow; (c) PT in both transforming regions completes and these zones coalesce (except for compression with torsion for $\sigma_{y2} = 0.2\sigma_{y1}$); (d) PT can be completed in almost the entire regions where $p > p_\varepsilon^d$ for torsion for any yield strength and for compression for $\sigma_{y2} = 0.2\sigma_{y1}$; (e) the magnitude of friction stresses τ in a single-phase region reaches a corresponding yield strength in shear in the major part of a sample; (f) for $\sigma_{y2} \neq \sigma_{y1}$, there is a sharp change in shear stresses τ_{rz} and $\tau_{r\varphi}$ at a diffuse interface.

More detailed analysis is summarized at the end of each section. Comparison with a simplified model and experiments is given in Secs. V and VI. The impact of our simulations on the possibility of complete or partial characterization of strain-induced PTs is discussed in Sec. VI.

Torsion significantly reduces the axial force (for the same pressure at the center) for complete PT for $\sigma_{y2} = \sigma_{y1}$, and especially for $\sigma_{y2} = 5\sigma_{y1}$, which is important if the experiment is conducted at the limit of anvil strength. However, the transformed region is smaller during the torsion, both due to a smaller region with $p > p_\varepsilon^d$ and a reduction in sample thickness during the torsion. When comparing at the same axial force, torsion allows one to drive PT to completion almost in the entire region with $p > p_\varepsilon^d$. Surprisingly, torsion suppresses PT for $\sigma_{y2} = 0.2\sigma_{y1}$, i.e., it reduces the volume of the fully transformed high-pressure phase, while only slightly reducing the axial force. Consequently, research on strain-induced PTs to a weaker phase does not require rotational anvils. It can be performed in traditional anvils, which drastically expands the opportunity for experimental studies on this phenomenon.

For the chosen volumetric transformation strain $\varepsilon_t = 0.1$ and kinetics, shear stress τ_{rz} does not change the sign, and there is no radial flow to the center of a sample. This result changes the generally accepted wisdom [based on Eq. (2)] that the maximum in pressure distribution corresponds to zero sliding radial velocity and that material flows radially in the direction of the pressure gradient.[10,12,13] For larger volumetric strain and faster kinetics, we may obtain radial flow to the center, as it was observed in experiments.[10]

The obtained results change the basic knowledge and intuition in interpretation of experimentally observed phenomena. They lead to better understanding of results of measurements and the methods of extracting of information on material constitutive equations from the sample behavior. They also represent a computational framework for designing experiments for various objectives and for controlling (promoting or suppressing) PTs for various applications, and they show the potential to completely characterize strain-induced PTs. Nontrivial effects are caused by multiple nonlinearities (due to large strains and material rotations, and nonlinearities in equations for plastic flow, PT kinetics, and contact friction) and by strong coupling between plasticity, PT, and contact friction.

Some of our conclusions are generic but some may change if a more sophisticated model or a different combination of material parameters is used. That is why in future work we will vary the kinetic coefficients (making them also different for direct and reverse PTs) and consider case $p_\varepsilon^r > p_\varepsilon^d$, when simultaneous direct and reverse PTs occur in a single material point (representative volume). In the direction of further development of the model, the kinetic equation that takes into account the effect of evolving defects on PT (see Ref. 6) will be utilized, and superposition of strain-induced and pressure-induced PT will be taken into account. Allowing for pressure dependence of the elastic properties and the yield strength, large elastic and transformation strains, deviatoric transformation strain, and transformation-induced plasticity and will further improve the model and the results. Unloading, torsion at a lower load when plastic flow does not start at the center of a sample during compression and complex compression-torsion-unloading-reloading history will be considered as well. Numerical treatment of the

contact problem for a sample with a gasket leading to a quasihomogeneous pressure distribution in a sample[6] will be performed with the goal of a developing robust method to extract PT kinetics from experiments.

*vlevitas@iastate.edu

[1] V. I. Levitas and O. M. Zarechnyy, preceding paper, Phys. Rev. B **82**, 174123 (2010).

[2] V. I. Levitas and O. M. Zarechnyy, Appl. Phys. Lett. **91**, 141919 (2007).

[3] V. I. Levitas and O. M. Zarechnyy, High Press. Res. (to be published).

[4] V. I. Levitas, *Large Deformation of Materials with Complex Rheological Properties at Normal and High Pressure* (Nova Science, New York, 1996).

[5] See supplementary material at http://link.aps.org/supplemental/10.1103/PhysRevB.82.174124 for distributions of normal and shear stresses in the sample and along its flat contact surface.

[6] V. I. Levitas, Y. Ma, J. Hashemi, M. Holtz, and N. Guven, J. Chem. Phys. **125**, 044507 (2006).

[7] V. D. Blank, Y. Y. Boguslavski, M. I. Eremetz, E. S. Izkevich, Y. S. Konyaev, A. M. Shirokov, and E. I. Estrin, Sov. Phys. JETP **87**, 922 (1984).

[8] N. V. Novikov, S. Polotnyak, L. Shvedov, and V. I. Levitas, J. Superhard Mater. **3**, 39 (1999).

[9] V. D. Blank, S. G. Buga, M. Y. Popov, V. A. Davydov, and V. Agafonov, New J. Chem. **19**, 253 (1995).

[10] V. D. Blank and S. G. Buga, Instrum. Exp. Tech. **36**, 149 (1993).

[11] S. S. Batsanov, N. R. Serebryanaya, V. D. Blank, and V. A. Ivdenko, Kristallografiya **40**, 650 (1995).

[12] V. I. Levitas, in *High Pressure Surface Science and Engineering*, edited by Y. Gogotsi and V. Domnich (Institute of Physics, Bristol, 2004), pp. 159–292.

[13] V. I. Levitas, Phys. Rev. B **70**, 184118 (2004).

[14] Y. Boguslavskii, K. Achmetshakirova, and S. Drabkin, Eur. Phys. J.: Appl. Phys. **3**, 243 (1998).

[15] G. B. Olson, in *Deformation, Processing and Structure*, edited by G. Krauss (ASM International, Warrendale, PA, 1984), pp. 391–424.

[16] M. M. Aleksandrova, V. D. Blank, and S. G. Buga, Solid State Physics **35**, 1308 (1993).

[17] V. D. Blank, Z. H. Malyushitska, and B. A. Kulnitskiy, High Pressure Physics and Technics **3**, 28 (1993).

[18] V. I. Levitas and O. M. Zarechnyy, J. Phys. Chem. B **110**, 16035 (2006).

[19] V. Domnich, D. Ge, and Y. Gogotsi, in *High Pressure Surface Science and Engineering*, edited by Y. Gogotsi and V. Domnich (Institute of Physics, Bristol, 2004), p. 381.

[20] V. I. Levitas, Y. Z. Ma, and J. Hashemi, Appl. Phys. Lett. **86**, 071912 (2005).

[21] Y. Ma, E. Selvi, V. I. Levitas, and J. Hashemi, J. Phys.: Condens. Matter **18**, 1075 (2006).

[22] Y. Z. Ma, V. Levitas, and J. Hashemi, J. Phys. Chem. Solids **67**, 2083 (2006).

Modeling and simulation of strain-induced phase transformations under compression and torsion in rotational diamond anvil cell

Valery I. Levitas[1][†] and Oleg M. Zarechnyy[2]

[1]*Iowa State University, Departments of Mechanical Engineering, Aerospace Engineering, and Material Science and Engineering, Ames, Iowa 50011, USA*

[2]*Iowa State University, Department of Aerospace Engineering, Ames, Iowa 50011, USA*
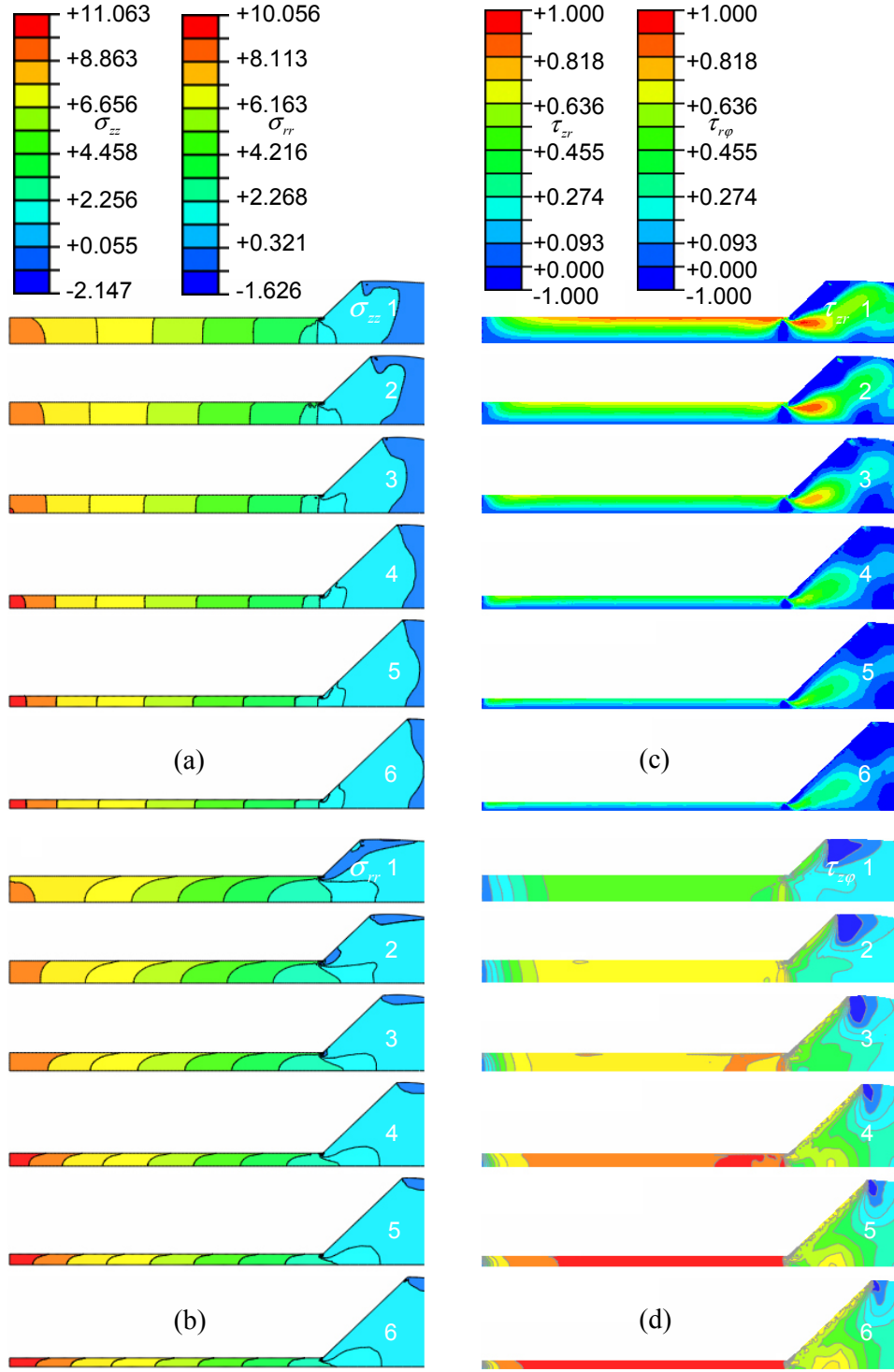
[†] e-mail: vlevitas@iastate.edu

FIG. S1. Distributions of normal stress σ_{zz} (a), normal stress σ_{rr} (b), shear stress τ_{zr} (c), and shear stress $\tau_{r\varphi}$ (d) for the case with $\sigma_{2y} = \sigma_{1y}$ for dimensionless applied axial force $F = 4.44$ and different values of angle of rotation φ. 1: $\varphi = 0.04$, 2: $\varphi = 0.14$, 3: $\varphi = 0.34$, 4: $\varphi = 0.78$, 5: $\varphi = 1.16$, 6: $\varphi = 1.58$.

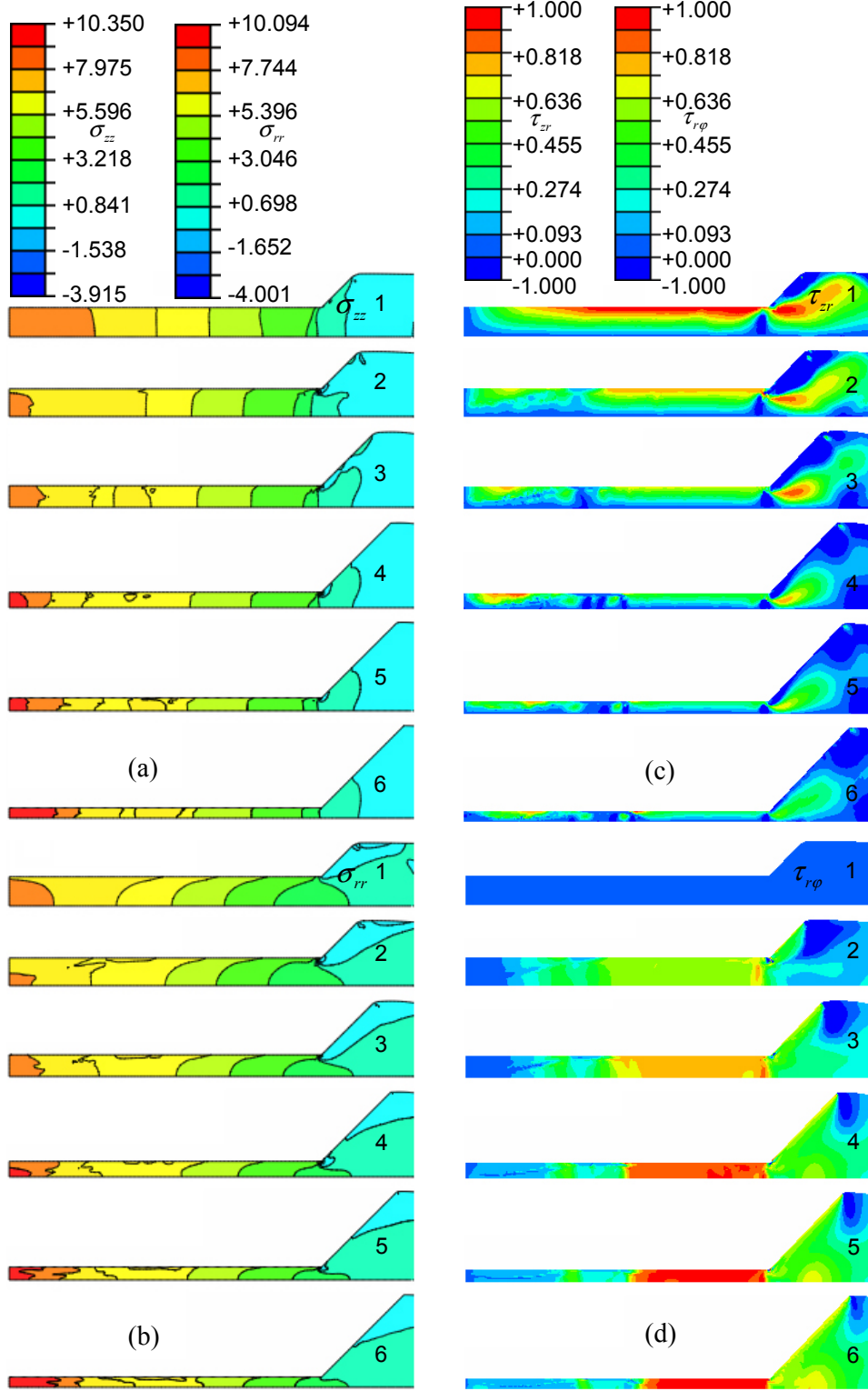FIG. S2. Distributions of normal stress σ_{zz} (a), normal stress σ_{rr} (b), shear stress τ_{zr} (c), and shear stress $\tau_{r\varphi}$ (d) in a quarter of cross section of the sample for the case with $\sigma_{2y} = 5\sigma_{1y}$ for dimensionless applied axial force $F = 4.44$ and different values of angle of rotation φ in a quarter of cross section of the sample.

1: $\varphi = 0.09$, 2: $\varphi = 0.38$, 3: $\varphi = 0.61$, 4: $\varphi = 0.94$, 5: $\varphi = 1.10$, 6: $\varphi = 1.30$.

FIG. S3. Distributions of normal stress σ_{zz} (a), normal stress σ_{rr} (b), shear stress τ_{zr} (c), and shear stress $\tau_{r\varphi}$ (d) in a quarter of cross section of the sample for the case with $\sigma_{2y} = 0.2\sigma_{1y}$ for dimensionless applied axial force $F = 4.44$ (except 1) and different values of angle of rotation. $1 : F = 4.30$, $\varphi = 0.0$, $2: \varphi = 0.09$, $3: \varphi = 0.20$, $4: \varphi = 0.64$, $5: \varphi = 0.84$, $6: \varphi = 1.40$.

FIG. S4. Distributions normal stress σ_{zz} (a) and normal stress σ_{rr} (b) along the radius of the contact surface of a sample r for the case with $\sigma_{2y} = \sigma_{1y}$ for dimensionless applied axial force $F = 4.44$ and different values of angle of rotation φ. 1: $\varphi = 0.04$, 2: $\varphi = 0.14$, 3: $\varphi = 0.34$, 4: $\varphi = 0.78$, 5: $\varphi = 1.16$, 6: $\varphi = 1.58$.
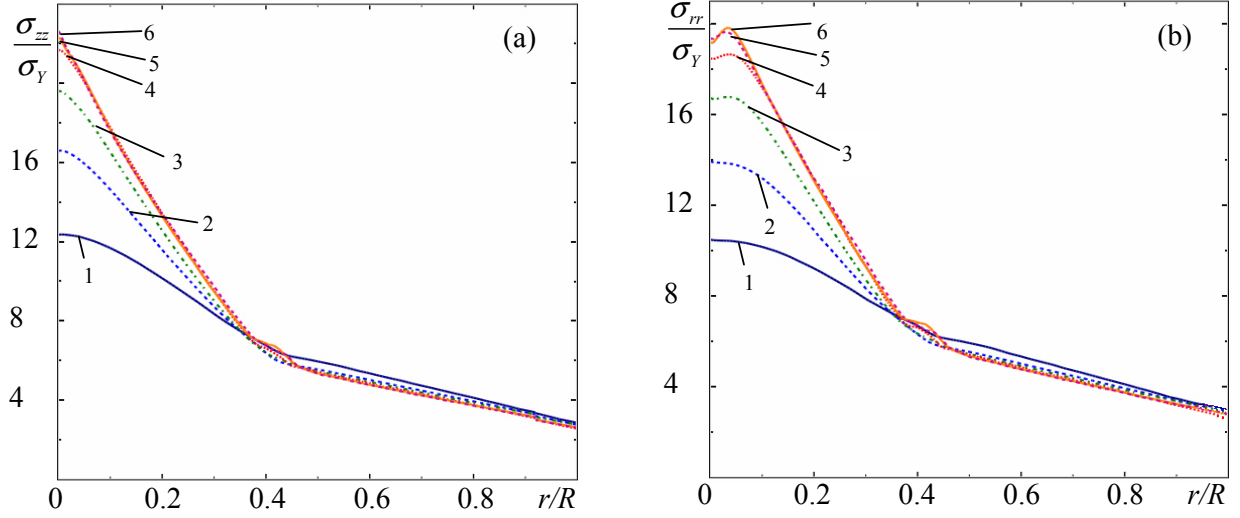
FIG. S5. Distributions normal stress σ_{zz} (a) and normal stress σ_{rr} (b) along the radius of the contact surface of a sample r for the case with $\sigma_{2y} = 5\sigma_{1y}$ for dimensionless applied axial force $F = 4.44$ and different values of angle of rotation φ. 1: $\varphi = 0.09$, 2: $\varphi = 0.38$, 3: $\varphi = 0.61$, 4: $\varphi = 0.94$, 5: $\varphi = 1.10$, 6: $\varphi = 1.30$.
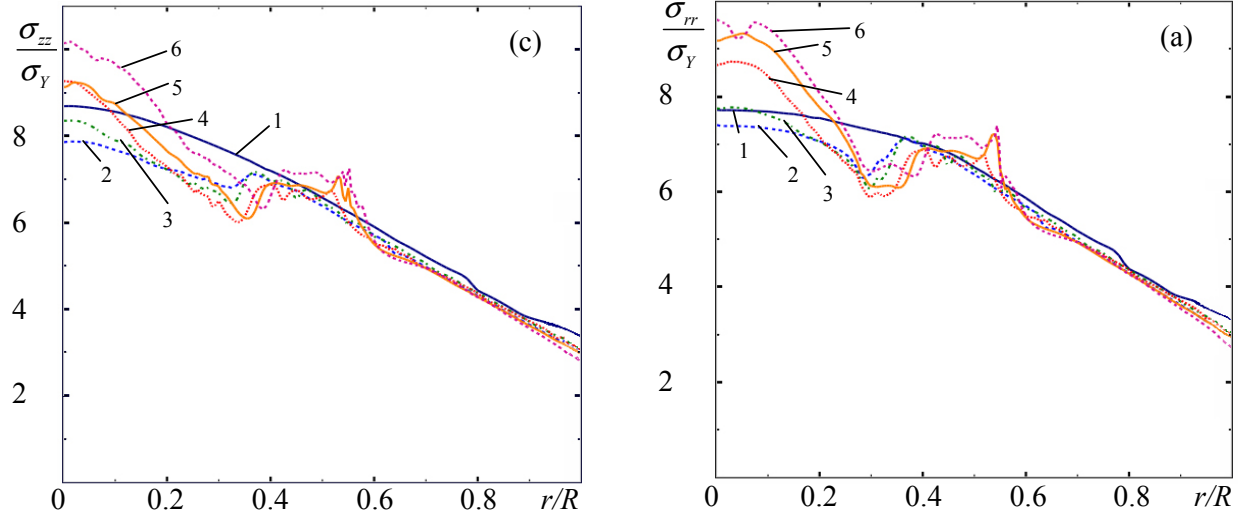
FIG. S6. Distributions normal stress σ_{zz} (a) and normal stress σ_{rr} (b) along the radius of the contact surface of a sample r for the case with $\sigma_{2y} = 0.2\sigma_{1y}$ for dimensionless applied axial force $F = 4.44$ and different values of angle of rotation φ. 1 : $F = 4.30$, $\varphi = 0.0$, 2: $\varphi = 0.09$, 3: $\varphi = 0.20$, 4: $\varphi = 0.64$, 5: $\varphi = 0.84$, 6: $\varphi = 1.40$.

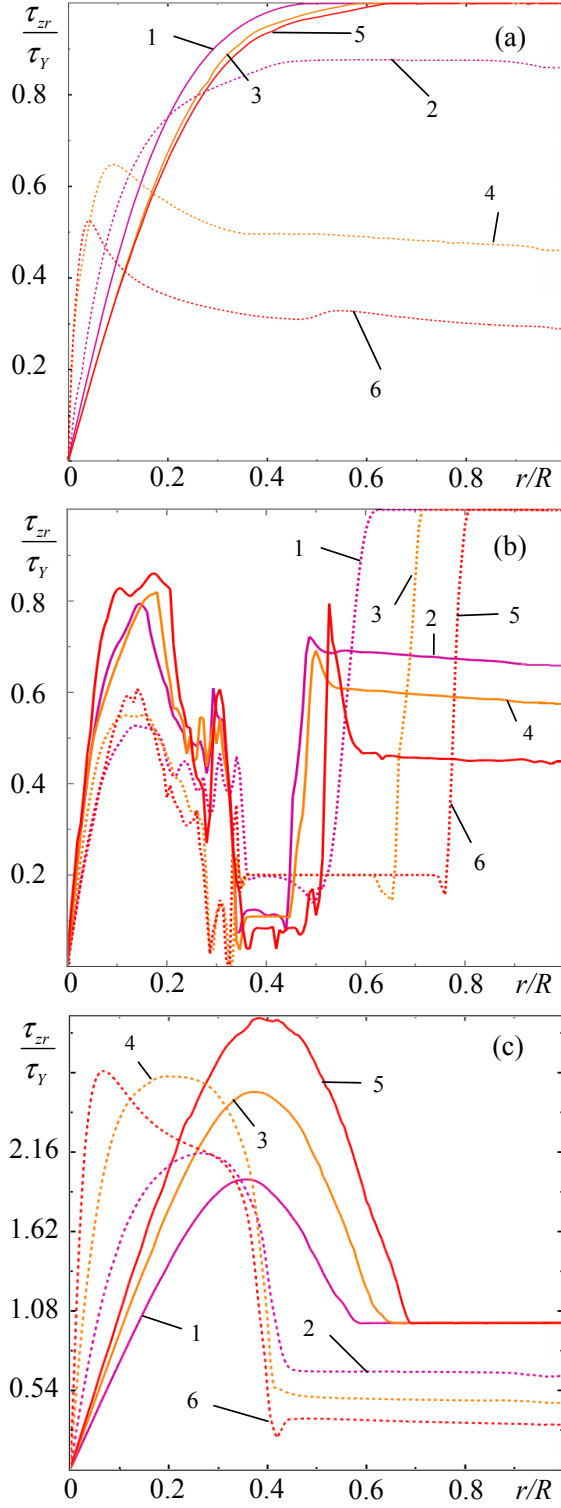FIG. S7. Comparison of shear stress τ_{zr} for compression (1, 3, 5) and torsion (2, 4, 6) for (a) $\sigma_{y2} = \sigma_{y1}$, the pressure at the contact surface at $r = 0$ after pure compression and torsion is the same and equal to 8.40 (1 and 2), 9.40 (3 and 4), and 10.2 (5 and 6). Dimensionless applied axial force F is 4.46 (1), 5.04 (3), 5.43 (5), and 4.44 (2, 4, 6). Rotation angle φ is 0.04 (2), 0.60 (4), and 1.57 (6).

(b) $\sigma_{y2} = 0.2\sigma_{y1}$, the pressure at the contact surface at $r = 0$ after pure compression and torsion is the same and equal to 7.95 (1 and 2), 8.10 (3 and 4), and 8.80 (5 and 6). Dimensionless applied axial force F is equal to 5.07 (1), 5.42 (3), 6.11 (5), and 4.44 (2, 4, 6). Rotation angle φ is equal to 0.20 (2), 0.32 (4), and 0.64 (6).

(c) $\sigma_{y2} = 5\sigma_{y1}$, the pressure at the contact surface at $r = 0$ after pure compression and torsion is the same and equal to 12.4 (1 and 2), 16.2 (3 and 4), and 20.1 (5 and 6). Dimensionless applied axial force F is equal to 5.47 (1), 6.26 (3), 7.21 (5), and 4.44 (2, 4, 6). Rotation angle φ is equal to 0.20 (2), 0.52 (4), and 1.11 (6).
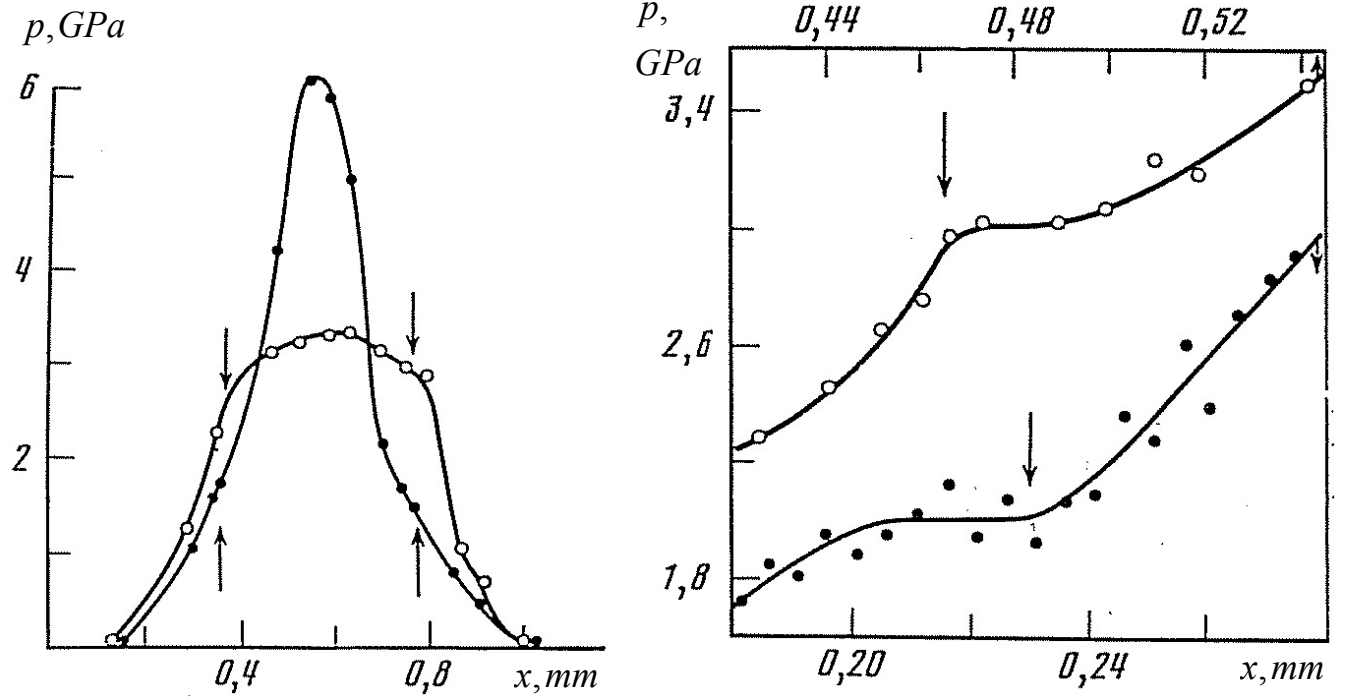
8

FIG. S8. Pressure distribution in KCL in the whole sample (left) and in the area of phase interface(right). ∘ line corresponds to the pure compression, • line corresponds to the compression with torsion. Arrows show phase interface (adopted from [7]).
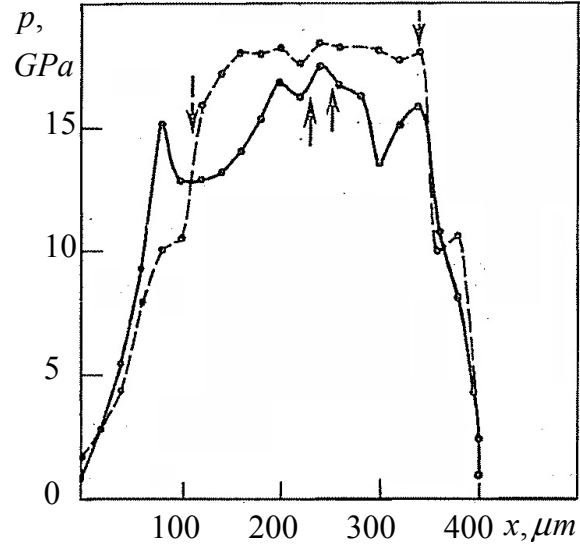
9

FIG. S9. Pressure distribution in $ZnSe$ sample before torsion (dashed line) and after torsion by 11°. Arrows show position of the phase interface (adopted from [10]).